Journal of Volcanology and Geothermal Research 444 (2023) 107940

Contents lists available at ScienceDirect

Journal of Volcanology and Geothermal Research

journal homepage: www.journals.elsevier.com/journal-of-volcanology-and-geothermal-research

Tectonically-determined distribution of monogenetic volcanoes in a compressive tectonic regime: An example from the Pannonian continental back-arc system (Central Europe)

Mátyás Hencz [a,b,*], Tamás Biró [b], Károly Németh [a,c,d], Kristóf Porkoláb [a], István János Kovács [e], Tamás Spránitz [a,f], Sierd Cloetingh [g], Csaba Szabó [a,f], Márta Berkesi [a]

[a] MTA-EPSS FluidsByDepth Lendület Research Group, Institute of Earth Physics and Space Science, Hungarian Research Network (HUN-REN), Sopron, Hungary
[b] Department of Physical Geography, Institute of Geography and Earth Sciences, ELTE Eötvös Loránd University, Budapest, Hungary
[c] National Program for Earthquakes and Volcanoes, Geohazard Research Center, Saudi Geological Survey, Jeddah, Saudi Arabia
[d] Istituto Nazionale di Geofisica e Vulcanologia, Bologna, Italy
[e] MTA-EPSS Lendület Pannon LitH$_2$Oscope Research Group, Institute of Earth Physics and Space Science, Hungarian Research Network (HUN-REN), Sopron, Hungary
[f] Lithosphere Fluid Research Lab, Institute of Geography and Earth Sciences, Eötvös Loránd University, Budapest, Hungary
[g] Tectonics Research Group, Department of Earth Sciences, Utrecht University, Netherlands

ARTICLE INFO

Keywords:
Bakony-Balaton Highland
Compression
Fault
GIS
Monogenetic
Lineament
Lithosphere

ABSTRACT

This paper presents the results from a geographic information systems (GIS) workflow, which was used to analyze the spatial distribution and temporal evolution of volcanoes in the Mio-Pleistocene monogenetic Bakony-Balaton Highland Volcanic Field (BBHVF), located in the Pannonian Basin, Hungary. Volcanism occurred during the tectonic inversion in a back-arc setting and a compressive/transpressive tectonic regime on the hottest and thinnest lithosphere of continental Europe. The main goal of this study is to clarify the effect of the pre-existing structure of the upper lithosphere in the distribution of the volcanic centers across the volcanic field using an innovative GIS methodology. Orientation of the volcanic field was compared to the orientation of the faults in the BBHVF, and in its larger vicinity, which resulted in correspondence, suggesting the dominance of the SW-NE direction. The directions of the volcanic lineaments fit well to the two main fault directions. The fault-volcano proximity analysis suggests that the fault plane of a thrust fault was an important structural feature during the lifespan of the volcanism. All results suggest that the fault plane of a regionally significant Cretaceous thrust fault (Litér Fault) might have served as a temporary pathway for the ascending magma, whereby (similarly to other, smaller faults) redirecting the magmas causing clustering of the volcanoes. This highlights the importance of major upper crustal structural heterogeneities for magma transport in a compressive tectonic system, especially in the case of active, monogenetic volcanic fields from a volcanic hazard perspective. The present GIS workflow can be effective in analyzing the spatial patterns of the volcanism and its connection with crustal structures at monogenetic volcanic fields worldwide.

1. Introduction

Monogenetic volcanoes, such as maars, tuff cones, tuff rings, scoria or cinder cones (Lorenz, 1986; Walker, 1993) are the most common type of subaerial volcanic landforms on Earth (Walker, 1993; Kereszturi and Németh, 2012; Tchamabé et al., 2016). These volcanoes can be described as short-lived (active from days to years), simple volcanic edifices fed by relatively small amount (<<2 km^3 in Dense Rock Equivalent - DRE) of magma (Walker, 1993; Valentine and Gregg, 2008). Such volcanoes can also be associated with compound, complex or shield volcanoes (collectively called as polygenetic volcanoes) on their flanks and/or situated on rift zones connected to them (e.g., Tenerife, Spain – Kereszturi et al., 2013; Etna, Italy – Corazzato and Tibaldi, 2006), but their "monogenetic" nature mostly manifests within their morphological and size parameters and not obviously with the magmatic plumbing system associated with them. However, their most

* Corresponding author at: MTA-EPSS FluidsByDepth Lendület Research Group, Institute of Earth Physics and Space Science, Hungarian Research Network (HUN-REN), Sopron, Hungary.
E-mail address: hencz.matyas@epss.hun-ren.hu (M. Hencz).

https://doi.org/10.1016/j.jvolgeores.2023.107940
Received 11 August 2023; Received in revised form 14 October 2023; Accepted 17 October 2023
Available online 19 October 2023

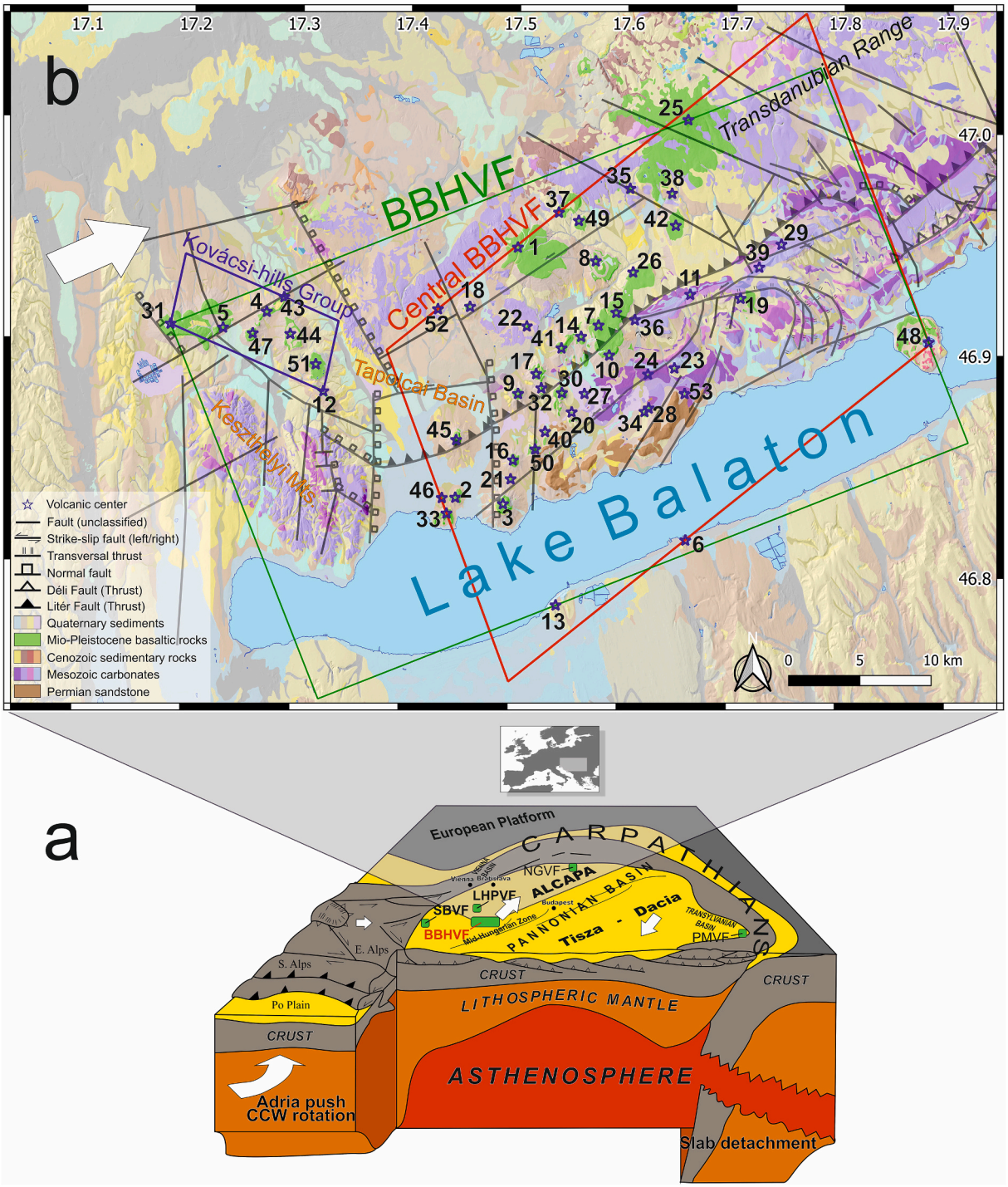

Fig. 1. a) 3D geodynamic environment of the BBHVF in the Carpathian-Pannonian region (CPR) (showing the ALCAPA (Alpine-Carpathian-Pannonian) and Tisza-Dácia microplates) during the basaltic volcanism, and the location of the main monogenetic basaltic volcanic fields in green polygons. BBHVF: Bakony-Balaton Highland Volcanic Field, LHPVF: Little Hungarian Plain Volcanic Field, SBVF: Styrian Basin Volcanic Field, NGVF: Nógrád-Gömör Volcanic Field, PMVF: Persany Mountains Volcanic Field. CCW: counterclockwise. White arrows show the directions of the movements based on Horváth and Cloetingh (1996) and Porkoláb et al. (2023). The figure is based on Horváth and Cloetingh (1996) and Cloetingh et al. (2010). b) Geologic map (https://map.mbfsz.gov.hu/fdt100/; Gyalog and Síkhegyi, 2005) of the Bakony-Balaton Highland Volcanic Field (BBHVF) with the volcanic centers (Table 1), main faults (e.g., Litér Fault – LF), and the bounding polygons (see details in text). Red: Central BBHVF, blue: Kovácsi-hills Group, green: whole BBHVF. Fault lines indicated by Budai et al. (1999b). (For interpretation of the references to colour in this figure legend, the reader is referred to the web version of this article.)

common manifestation (sensu stricto) are stand-alone volcanic fields consisting of number of individual monogenetic volcanoes. These monogenetic volcanic fields contain several dozens to several hundreds of eruption centers scattered among the area, physically appearing as small cones, maars, and associated widespread lava flows (D'Orazio et al., 2000; Rodríguez et al., 2010; Brenna et al., 2011). Intra-continental monogenetic basaltic volcanic fields are commonly formed in extensional/transtensional tectonic setting (such as South Auckland Volcanic Field in New Zealand; Cook et al. (2005) or Snake River Plain in Idaho, USA; Hughes et al. (2002)). In contrast, there are only a few

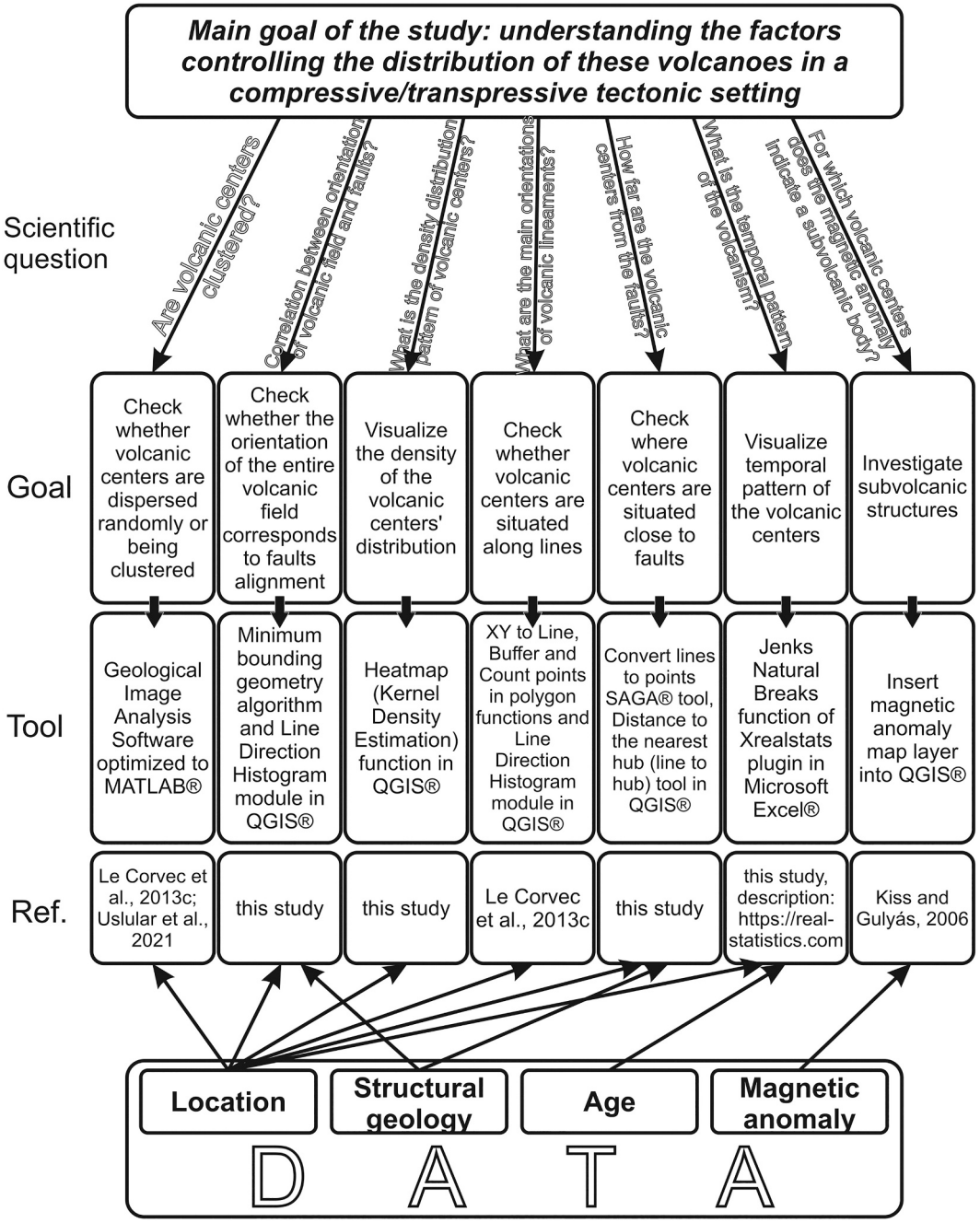

Fig. 2. Summary flowchart of the GIS or statistical methodology used. Detailed technical information about each workflow can be found in Appendix A.

situated in convergent tectonic regime or in compressional/transpressional stress field (e.g., Abu Monogenetic Volcano Group, Japan – Kiyosugi et al., 2010; Mojave Desert area, California, USA – Glazner and Bartley, 1994; Tibaldi et al., 2009; Northern Chile – Ureta et al., 2020, 2021a, 2021b). Horizontal shortening does not favor the ascending of magma towards the surface; nevertheless, reverse faults can facilitate the ascent of magma as well. (Tibaldi et al., 2009). Tectonic regime is used here as a regional term, many different local aspects and expressions can occur. For example, the Kamo Volcanic Field, southern Kyusu, Japan, where the tectonic regime along the Japan arc is compressional, but localized extension or asymmetric variations of extension-compression are common and may open the way to form volcanoes (Nche et al., 2021).

By analyzing of spatial aspects of a volcanic field (Abu Monogenetic Volcano Group, Japan, Kiyosugi et al., 2010; Auckland Volcanic Field, New Zealand, Le Corvec et al., 2013a; Los Tuxtlas Volcanic Field, Mexico, Sieron et al., 2021), knowledge can be acquired on the relationships between the basaltic magmatism and regional tectonics, like impact of faults to the position of the volcanoes, vent propagation in the lithosphere, or age-dependent stress condition changes (Connor et al., 1992; Tadini et al., 2014; Cañon-Tapia, 2021). Recent studies have been identified non-random patterns in the spatial distribution of the volcanic eruption centers among volcanic field using different mathematical and statistical approaches (e.g., Magill et al., 2005; von Veh and Németh, 2009; Kiyosugi et al., 2010, 2012; Rodríguez et al., 2010; Le Corvec et al., 2013a, 2013b; Kereszturi et al., 2014). The main outcome of these recent studies has been established statistically validated alignments and clusters in the distribution of volcanoes, which corresponds well with the larger-scale lithosphere structure or regional tectonic features (Marett and Emerman, 1992; Kiyosugi et al., 2010; Martí et al., 2016).

Table 1
All volcanic centers (with decimal coordinates) recognized in the BBHVF, and available ages are listed based on recent publications. The volcanic centers are depicted in Fig. 1b with the numbers shown in the first column. [1] data based on Balogh et al. (1982, 1986); Borsy et al. (1987); Balogh and Pécskay (2001); Balogh and Németh (2005); and Kereszturi et al. (2011); [2] data based on Wijbrans et al. (2007), n.d.: no data. Ar-Ar ages were used where were available, if not, then K-Ar ages were used.

Nr.	Volcanic center	Lat (°)	Lon (°)	K-Ar age (Ma) [1]	Ar-Ar age (Ma) [2]	The age used in this study	Age group (see Section 4.7)
1	Agár-tető	46.964	17.502	2.98 ± 0.18	3.00 ± 0.03	3.00	1
2	Antal-hegy (Szigliget)	46.805	17.449	4.17 ± 0.37	n.d.	4.17	3
3	Badacsony	46.802	17.493	3.45 ± 0.23	n.d.	3.45	2
4	Bazsi	46.920	17.272	3.27 ± 1.70	n.d.	3.27	2
5	Bercehát	46.909	17.232	n.d.	n.d.	–	–
6	Boglár	46.781	17.661	n.d.	n.d.	–	–
7	Boncsos-tető	46.915	17.577	2.97 ± 0.11	n.d.	2.97	1
8	Bondoró	46.956	17.574	2.57 ± 0.26	n.d.	2.57	1
9	Csobánc	46.871	17.505	3.42 ± 0.41	n.d.	3.42	2
10	Fekete-hegy	46.897	17.588	3.98 ± 0.34	3.81 ± 0.02	3.81	2
11	Fenyves-hegy	46.936	17.661	n.d.	n.d.	–	–
12	Fertős-hegy	46.870	17.325	n.d.	n.d.	–	–
13	Fonyód	46.738	17.543	3.55 ± 0.90	n.d.	3.55	2
14	Füzes-tó	46.908	17.562	n.d.	2.61 ± 0.03	2.61	1
15	Gajos-tető (Fekete-hegy)	46.924	17.593	3.82 ± 0.17	n.d.	3.82	2
16	Gulács	46.829	17.501	3.66 ± 0.14	n.d.	3.66	2
17	Hajagos	46.884	17.521	3.94 ± 0.25	3.80 ± 0.02	3.8	2
18	Haláp	46.926	17.459	2.94 ± 0.34	3.06 ± 0.02	3.06	1
19	Halom-hegy	46.934	17.708	3.26 ± 0.13	4.08 ± 0.05	4.08	3
20	Harasztos-hegy	46.860	17.554	3.50 ±?	n.d.	3.5	2
21	Hármas-hegy	46.817	17.499	n.d.	n.d.	–	–
22	Hegyesd	46.914	17.511	3.43 ± 0.22	4.12 ± 0.01	4.12	3
23	Hegyes-tű	46.889	17.648	5.97 ± 0.41	7.94 ± 0.03	7.94	5
24	Horog-hegy	46.885	17.624	n.d.	n.d.	–	–
25	Kab-hegy	47.046	17.657	5.23 ± 0.58	n.d.	5.23	4
26	Kecske-hegy (Fekete-hegy)	46.949	17.608	4.66 ± 0.36	n.d.	4.66	3
27	Kereki-hegy	46.872	17.566	n.d.	n.d.	–	–
28	Kis-Hegyes-tű	46.862	17.621	n.d.	n.d.	–	–
29	Kőhegy	46.968	17.745	5.69 ± 0.31	n.d.	5.69	4
30	Kopasz-hegy	46.872	17.545	2.82 ± 0.36	n.d.	2.82	1
31	Kovácsi-hegyek	46.911	17.183	3.10 ± 0.26	n.d.	3.1	1
32	Köves-hegy	46.875	17.526	n.d.	n.d.	–	–
33	Külső-hegy (Szigliget)	46.795	17.441	3.87 ± 0.28	4.53 ± 0.05	4.53	3
34	Lapos-Hegyes-tű	46.864	17.625	n.d.	n.d.	–	–
35	Öcs-hegy	47.002	17.604	n.d.	n.d.	–	–
36	Öreg-hegy	46.919	17.611	n.d.	n.d.	–	–
37	Pénzes-kő (Taliándörögd)	46.986	17.539	4.50 ±?	n.d.	4.5	3
38	Pula maar	46.999	17.643	4.25 ± 0.17	n.d.	4.25	3
39	Ragonya	46.954	17.725	7.92 ± 0.33	n.d.	7.92	5
40	Sabar-hegy	46.848	17.530	n.d.	n.d.	–	–
41	Sátorma-hegy	46.901	17.544	4.09 ± 0.18	n.d.	4.09	3
42	Som-hegy (Tálodi-erdő)	46.979	17.647	4.65 ± 0.72	n.d.	4.65	3
43	Sümegprága	46.929	17.288	3.34 ± 0.23	4.15 ± 0.05	4.15	3
44	Szebike	46.906	17.294	n.d.	n.d.	–	–
45	Szent György-hegy	46.841	17.448	3.35 ± 0.25	4.22 ± 0.04	4.22	3
46	Vár-hegy (Szigliget)	46.805	17.436	3.30 ± 0.21	4.08 ± 0.02	4.08	3
47	Tátika	46.906	17.259	3.34 ± 0.18	n.d.	3.34	2
48	Tihany	46.908	17.882	7.54 ± 0.50	7.96 ± 0.03	7.96	5
49	Tik-hegy	46.981	17.557	n.d.	n.d.	–	–
50	Tóti-hegy	46.836	17.521	5.71 ± 0.29	4.74 ± 0.02	4.74	3
51	Uzsa	46.887	17.318	3.83 ± 0.65	n.d.	3.83	2
52	Véndek-hegy	46.924	17.429	n.d.	n.d.	–	–
53	Zánkai Várhegy	46.873	17.658	n.d.	n.d.	–	–

This demonstrated that the exact spots and the timing where and when magma reaches the surface are controlled by regional stress conditions and/or pre-existing fractures of the basement (e.g., Connor, 1990; Connor et al., 1992; Valentine and Perry, 2007; Le Corvec et al., 2013c; Tadini et al., 2014). Fractures may serve as pathways for the melt on its way to the surface, leading to the grouping of the volcanoes along these pathways (Gaffney et al., 2007; Le Corvec et al., 2013b). However, these results should be evaluated carefully, since there are other important factors which may affect vent alignments (e.g., melting extent, local stress fields, etc.; Cañon-Tapia, 2021). Investigation of geological structure and spatial distribution of volcanoes on active monogenetic volcanic fields is important from the perspective of volcanic hazards, because understanding the spatial and temporal pattern of the volcanism may improve capabilities concerning the place and time of a future eruption (Magill et al., 2005; Valentine and Perry, 2007; Le Corvec et al., 2013a). It is also essential to know these features of ancient, inactive monogenetic volcanic fields to obtain a comprehensive assessment of the whole lifespan of volcanic fields, especially the types and temporal dimensions of the eruptions. The geologically validated analogies need to be considered for future eruptions of active volcanic fields in terms of spatially, temporally, and process-oriented, deterministic approaches (Martin et al., 2003; Magill et al., 2005; Kereszturi et al., 2014).

In this paper, a GIS-based study was conducted on a Mio-Pleistocene monogenetic basaltic volcanic field (Bakony-Balaton Highland Volcanic Field, Hungary – BBHVF hereafter) formed in the post-rift phase of the Carpathian-Pannonian region (CPR) evolution, where the basaltic volcanic paroxysm is coeval with the onset of tectonic inversion, 8–5 Ma (Balázs et al., 2016; Kovács et al., 2020). Yet, understanding the factors controlling the distribution of these volcanoes in a predominantly compressive/transpressive tectonic setting remains a profound

challenge (Martin et al., 2003; Jankovics et al., 2013; Harangi et al., 2015; Kovács et al., 2020). The main goal of the study is understanding the factors controlling the distribution of these volcanoes in a compressive/transpressive tectonic setting. Here the volcano distribution, as well as their correlation with structural geology of the country rocks are investigated (using kernel density distribution map, calculated distances from faults, orientation of the volcanic field, etc.) in order to better understand how the lithospheric structure controlled the distribution of volcanoes. Age clustering of the volcanoes is also considered to analyze any temporal pattern of the volcanism.

2. Geological background

2.1. Geodynamic and geological environment

The BBHVF (CPR, Central Europe) is an intracontinental monogenetic volcanic field (Németh and Martin, 1999; Martin et al., 2003; Kereszturi et al., 2011) developed between 7.96 and 2.61 Ma (Balogh et al., 1986; Borsy et al., 1987; Balogh and Németh, 2005; Wijbrans et al., 2007), and consists of at least 53 deeply eroded 1) basaltic monogenetic volcanoes (such as maars, tuff rings, scoria cones; Németh and Martin, 1999; Martin et al., 2003; Hencz et al., 2017) and 2) volcanoes considered to have more polygenetic affinity (e.g., shield volcanoes with multiple capping scoria cone(s); Németh and Martin, 1999; Martin and Németh, 2004). The BBHVF was active in the post-rift phase of the evolution of the Pannonian Basin, which started at about 11 Ma (Fig. 1a, Matenco et al., 2003). The melt was originated from a 'wet' asthenosphere based on structural hydroxyl content of mantle-derived clinopyroxene megacrysts in alkaline basalts (Szabó et al., 1992, 2004; Embey-Isztin et al., 1993; Kovács et al., 2020).

The basement of the Transdanubian Range, where the BBHVF is located, consists of a basal low-grade metamorphic Paleozoic succession, overlain by a non-metamorphic Permo-Mesozoic succession, made up by Permian red sandstone, and capped by regionally widespread Mesozoic carbonates (limestones, dolomites, marls) (Budai et al., 1999a). These are partly covered by the Miocene sand, clay or marl accumulated within a large lacustrine system across Central Europe named as Lake Pannon. In addition, young Pleistocene and Holocene diluvial, alluvial deposits, loess and various gravitational mass movement deposits complete the geological architecture of the region (Fig. 1b). The Mesozoic carbonates are exposed in the northern and south-eastern part of the BBHVF, whereas Paleozoic rocks are found in the southern part of the study area, just north of the shore of Lake Balaton (Fig. 1b). The volcanic remnants are emplaced directly on the Mesozoic carbonates, or on the Pannonian sediments, especially in the central part of the BBHVF (Martin and Németh, 2004). The main volcanic architectures (maars and tuff rings; Németh and Martin, 1999; Martin et al., 2003) were formed via phreatomagmatic eruptions (Sheridan and Wohletz, 1983; Lorenz, 1986). The external water, which was necessary to fuel for the phreatomagmatic fragmentation of the rising magma, was supplied by the water-rich Pannonian sediments and/or the Mesozoic carbonates depending on their availability (Németh and Martin, 1999; Martin et al., 2003; Kereszturi et al., 2011). At later stage of the eruptions, the maar and tuff ring craters were commonly filled by lava forming lava lakes in some cases, or the crater capped by a scoria cone (Martin and Németh, 2004).

The geomorphological picture of the BBHVF can be described as a basin, where the deeply eroded volcanic edifices protruding from the surface and forming hills via geomorphological inversion, because most commonly the upper or lower diatremes are on the surface in form of plugs (e.g., Hegyestű) and buttes (e.g., Badacsony; Németh and Martin, 1999). Shield volcanoes (Kab-hegy, Agár-tető; Martin and Németh, 2004) are situated at the north of the BBHVF, and their primary volcanic shape dominates the landscape (Fig. 1b).

The BBHVF are separated into two parts: a central part (Central BBHVF hereafter), which is situated in the vicinity of the Lake Balaton (including its southern shoreline), and a northwestern part, classified into Keszthelyi Mountains (Csorba, 2021), and represented by subvolcanic basaltic bodies (sill- and dyke-system) and exhumed diatreme (s) of maar volcanoes (Martin and Németh, 2004; Németh and Martin, 2007). The latter is named as Kovácsi-hills Group in this work for simplicity after a famous touristic spot of this area. In many publications the Little Hungarian Plain Volcanic Field (LHPVF) is discussed together with BBHVF (e.g., Martin and Németh, 2004; Kovács et al., 2020), but in this work the large distance (tens of kilometers) makes unjustified to include it to the spatial investigation accepting the fact that the two fields cannot be separated from a petrogenetical or volcanological point of view (e.g., Martin and Németh, 2004; Jankovics et al., 2015).

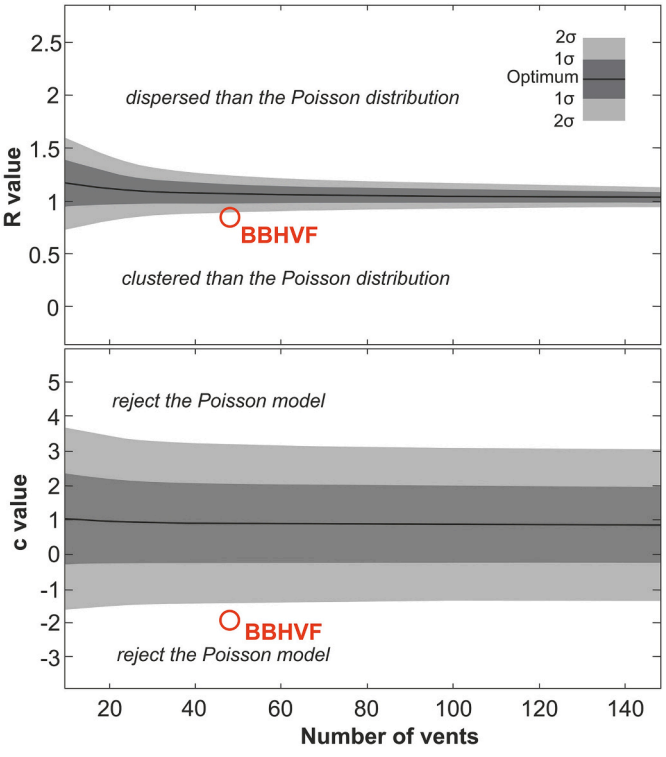

Fig. 3. Number of vents vs. statistical values of R and c plots. The Poisson model is not true for BBHVF, thus showing a clustered volcanic centers' distribution characteristic.

2.2. Structural setting

The Transdanubian Range (Fig. 1b) tectonic unit represents the uppermost part of the Cretaceous ("eoalpine") nappe stack of the Eastern Alps (e.g., Tari, 1994; Schmid et al., 2008). Cretaceous deformation of the Transdanubian Range resulted in map-scale folds and reverse faults (thrusts) striking in general NE–SW (e.g., Tari, 1994; Tari and Horváth, 2010; Csicsek and Fodor, 2016). The most prominent Cretaceous structure (Kókay, 1976) is the so-called Litér (thrust) Fault (LF hereafter, Fig. 1b), which is striking NE-SW, and separates an anticline in the north as hanging wall from a syncline as footwall in the south (Fig. 1b; e.g., Budai et al., 1999a; Csicsek and Fodor, 2016). Structural observations imply that significant reverse-sense slip on the LF did not occur following the Cretaceous nappe stacking. In contrast, the Miocene extension of the Pannonian Basin (Fig. 1a) induced minor normal-sense reactivation of some segments of the LF between ca. 12–8 Ma (Fodor et al., 2017; Visnovitz et al., 2021). By the end of the Miocene, the extensional/transtensional stress field changed to compressional/transpressional (Tari, 1994; Fodor et al., 2017), with a generally NE-SW compression and shortening direction (subparallel with the LF) that is still characteristic nowadays (Fig. 1a; Fodor et al., 1999; Bada et al.,

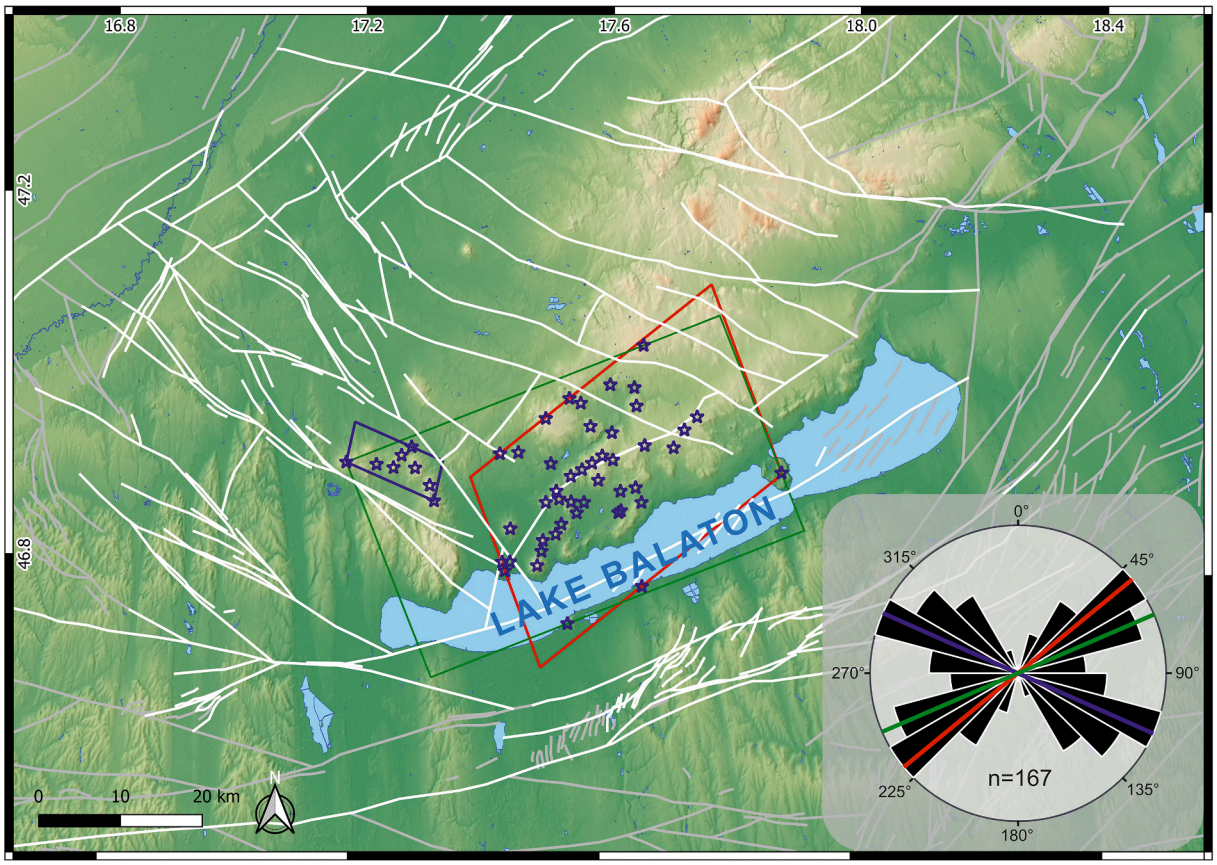

Fig. 4. Map about the BBHVF and adjacent areas and faults based on Wórum et al. (2020) and Koroknai et al. (2020) with white solid lines. Note that the distant faults are shown as grey solid lines. Bounding polygons are similar to those presented in Fig. 1b. Rose diagram showing the orientations of all faults visualized in the map with black, and with solid lines the orientation of the longer side of the bounding rectangles. Red: Central BBHVF, blue: Kovácsi-hills Group, green: whole BBHVF. n: number of the faults which directions are depicted in the rose diagram. Faults with grey solid lines are not used for direction calculations. (For interpretation of the references to colour in this figure legend, the reader is referred to the web version of this article.)

2007; Békési et al., 2023; Porkoláb et al., 2023). This renewed compression led to the inversion of the Pannonian Basin (e.g., Tari, 1994; Horváth and Cloetingh, 1996; Fodor et al., 1999), and resulted in minor strike-slip motions in the region of the Transdanubian Range, including minor sinistral slip along eastern segment of the LF (Visnovitz et al., 2021). The lack of significant post-Miocene faulting in the area of the BBHVF is also demonstrated by the correlation of Late Miocene-Pliocene paleosurface horizons between the volcanic edifices: paleosurfaces have gentle dip and show no major jumps related to fault activity (Fodor et al., 2022).

3. Methods

In this study, the main goal was to recognize patterns in the distribution of the volcanoes of the BBHVF. Firstly, the orientation of the volcanic field (considered as a whole; defined by the bounding polygon) was established. Then, the spatial density of the eruption centers was calculated. Volcanic lineaments were calculated using a multi-step GIS workflow including database construction using Python® and spatial analysis within QGIS® (version 3.16) to provide quantitative description of the link between the regional geological structures and the position of the volcanoes. The distance of the volcanoes from the nearest tectonic fault was also calculated. All available age data were collected and were included in a database. To recognize the gaps and cycles in the volcanism regarding time constraints, spatial distribution or clustering of the identified age groups were investigated. All technical details can be found in Appendix A, and in a summarizing flowchart about the methodology (Fig. 2).

4. Results

4.1. Establishing volcanic centers and corresponding ages

Localization of all eruption centers in an ancient volcanic field like the BBHVF remains a challenge: there are many well-visible, butte-like edifices, although sometimes only a few blocks of pyroclastic debris are indicating the location of minor eruption centers eroded to their roots (e.g., Németh, 2010). All possible eruption centers from old (e.g., Jugovics, 1968) and recent studies (e.g., Németh and Martin, 1999; Martin and Németh, 2004) were obtained (Table 1). In some cases, the exact number of eruption centers were not identified and located, because different, discordantly capping pyroclastic units can be seen in the field. Moreover, appropriate dating results are not able to tell the temporal context between them. For example, at Tihany (Fig. 1b), where at least three vents are located based on physical volcanological observations (Németh et al., 2001), however their magmatic relation could not be established due to lack of in-depth geochemical studies. In addition, inactive periods lasting for several thousand years cannot be inferred between the activity of the three vents. In the case of Szigliget (Fig. 1b), at least three deeply eroded diatreme structures are cropping out based on different dating methods (Table 1; called here as Vár-hegy, Külső-hegy, Antal-hegy), and physical volcanological investigations (Németh et al., 2000). However, at Tihany there is only one Ar-Ar age (7.96 Ma; Table 1; Wijbrans et al., 2007) available for the pyroclastic rocks (Tihany – Belső-tó), thus it is needed to handle Tihany as one eruption center with 3 closely-related vents (Németh et al., 2001).

The locations of individual eruption centers were marked manually

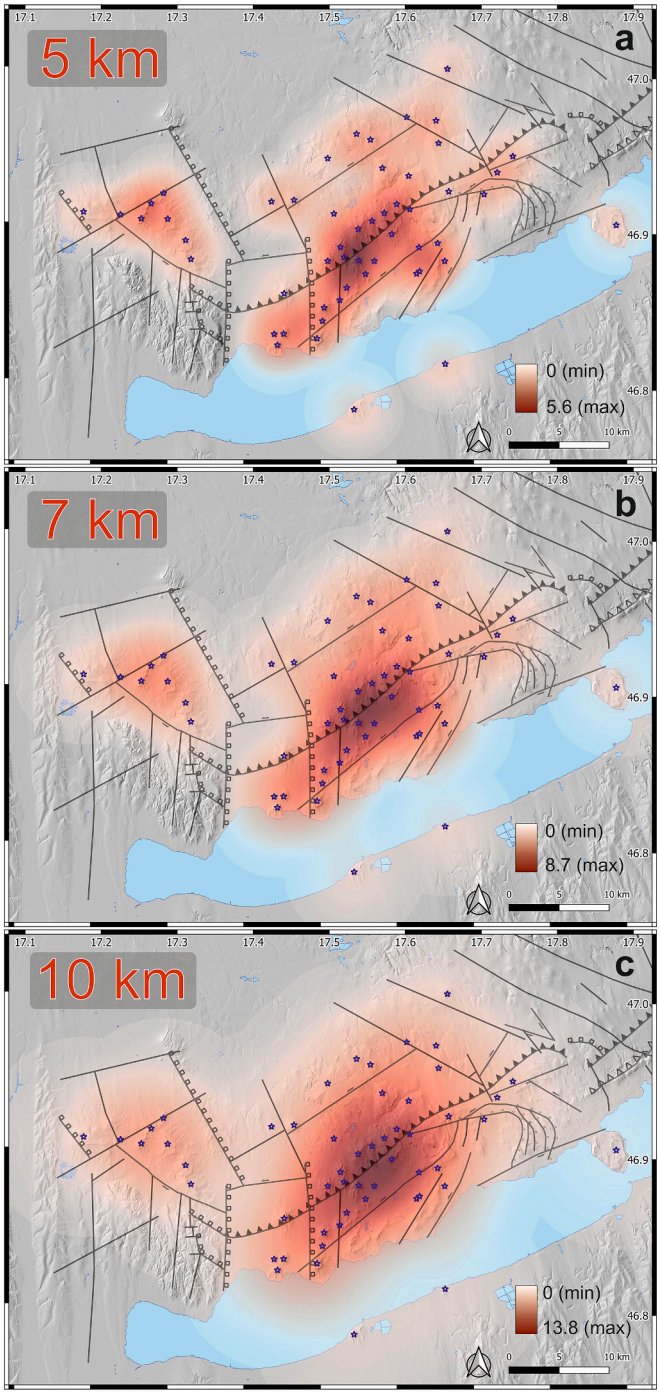

Fig. 5. Heatmap (kernel density distribution map) of the volcanic centers of the BBHVF. As darker the red as densest the volcano distribution. The different searching radii are indicated at the top left corner (a-c). Fault lines indicated by Budai et al. (1999b). (For interpretation of the references to colour in this figure legend, the reader is referred to the web version of this article.)

to the former center of the volcanoes as accurately as possible (Fig. 1b, Table 1). It has to be highlighted that Lake Balaton (formed in the Holocene) potentially covers many volcanic centers or subvolcanic bodies today (Balázs et al., 2011), which were omitted from present study because of the great uncertainty about their existence.

Traditional K-Ar ages were obtained for most of the eruption centers previously (Table 1; Balogh et al., 1986; Borsy et al., 1987; Balogh and Németh, 2005). However, in most cases, significant K or Ar loss is evident (Wijbrans et al., 2007). Thus, Ar-Ar dating was carried out later for several eruption centers (Wijbrans et al., 2007, see Table 1). In our investigation, Ar-Ar ages were prioritized over K-Ar ages in case available.

4.2. Nearest neighbor (NN) analysis

The spacing and clustering of vents is an important feature for understanding the crustal mechanisms forcing distribution of volcanic centers (Mazzarini, 2007; Uslular et al., 2021). Nearest neighbor analysis (Clark and Evans, 1954) is commonly used to quantify the spatial distribution of point-like features, like volcanic centers (Le Corvec et al., 2013c; Mazzarini et al., 2016; Uslular et al., 2021). More precisely, Poisson nearest neighbor analysis (PNN) as a type of NN methodology, is commonly used in case of volcanic fields for this (Le Corvec et al., 2013c). The PNN analysis provides useful information on the spatial distribution of vents and how this is related to our interpretation and inferences on the role of faults in providing pathways for magmatic transport. In this context, it is crucial to statistically assess the randomness of the distribution of the volcanoes. If the spatial distribution of volcanoes were statistically completely random, there would be no need for investigating the controls of faults on volcanism in this area. For technical details see Appendix A/1. R and c statistical parameters are presented in Fig. 3. These values, similar to the coefficient of variation used in Mazzarini and Isola (2010) allows to describe the homogeneity in the volcanoes' distribution, i.e., whether the spatial distribution is random, or rather showing clusters. In a hypothetical idealized case, R and c values for a population showing Poisson distribution are 1 and 0, respectively, i.e., in this case, the eruption centers are randomly distributed in space (cf. Miller, 2015). When the distribution is more 'random' relative to Poisson, R values will be larger than 1, whereas if the eruption centers are more clustered, R values will be smaller than 1 (Beggan and Hamilton, 2010). Values of R and c are plotted with the confidence interval of 2σ due to their sample size-dependence, to assess the suitability of the PNN analysis (Fig. 3, Le Corvec et al., 2013c).

The PNN analysis of the vents of BBHVF do not fit the Poisson model (Fig. 3). The c value falls outside the 2σ optimal value of the Poisson model ($c = -1.94$), whereas the R value suggests a clustered vent distribution than the Poisson distribution ($R = 0.85$). Thus, volcanoes show rather clustered than a random spatial distribution. Overall, PNN analysis demonstrates that volcanic centers have a clustered spatial distribution. This is the motivation to examine the impact of upper crustal structures on magma emplacement.

4.3. Orientation of the volcanic field compared to the main faults

The result of the orientation examination of the volcanic field is visualized in Fig. 4. For this method, BBHVF was segmented into two parts: Central BBHVF (red polygon in Figs. 1b and 4) and Kovácsi-hills Group (blue polygon in Figs. 1b and 4). A bounding polygon was also created for the whole BBHVF (green rectangle in Figs. 1b and 4). We used the fault lines based on literature data and reflection seismic data (white solid lines in Fig. 4; Koroknai et al., 2020; Wórum et al., 2020). This was the most recently published dataset, which is available for the larger vicinity of the BBHVF (in other cases, structural geological map of Budai et al. (1999b) was used because it is fit for the BBHVF itself). The furthest faults are filtered out (see the NW or SE part of the map in Fig. 4). Technical details can be found in Appendix A/2.

Direction of faults showing two main orientations: ENE-WSW, and WNW-ESE. Similarly to the former, the orientation of the whole BBHVF is ENE-WSW (Fig. 4). The central BBHVF is NE-SW oriented, whereas the Kovácsi-hills Group is showing a WNW-ESE orientation. Directions of the bounding geometries correspond well with the most typical directions of the faults.

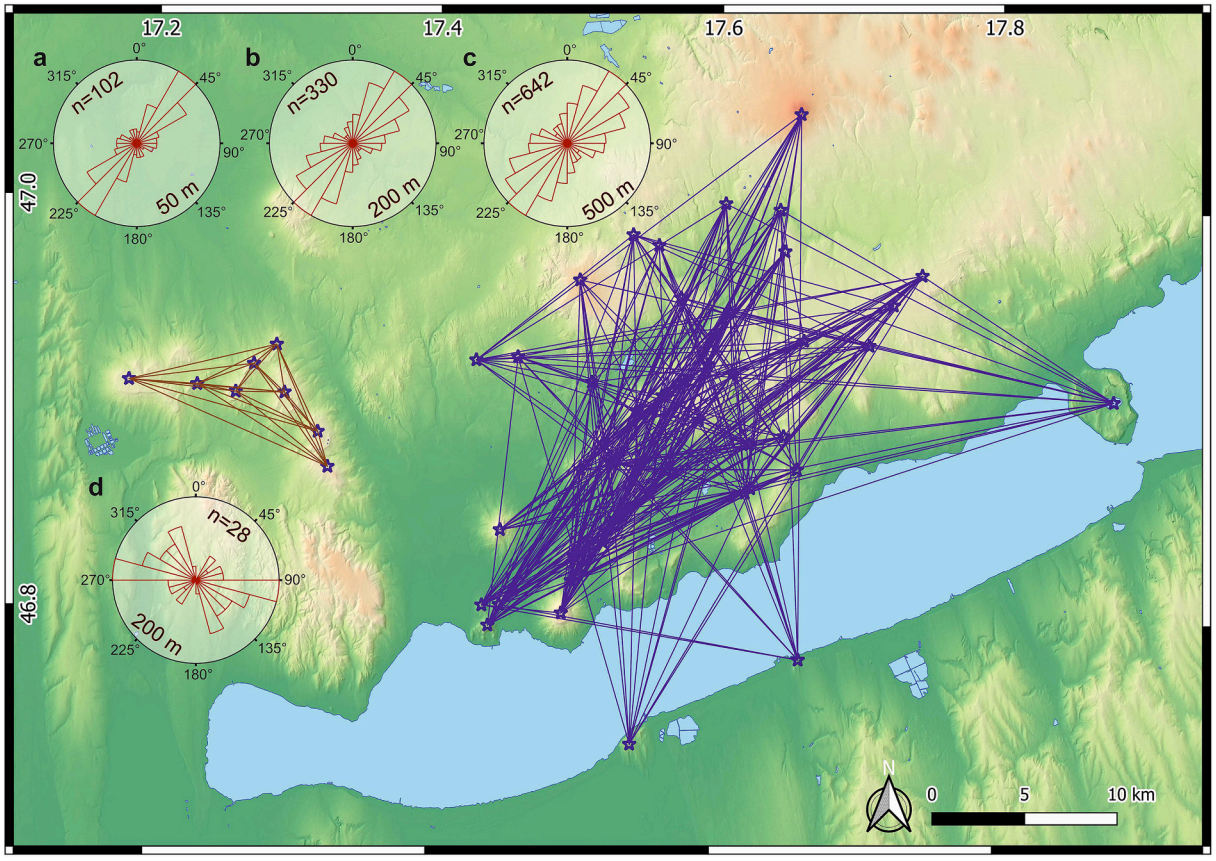

Fig. 6. The map shows the obtained volcanic lineaments in cases when there are at least 3 volcanoes in a line including the tolerance zone of 200 m. Results of other tolerance zones are not depicted, only used for rose diagrams. Rose diagrams show the orientation of volcanic lineaments. The used tolerance zone is indicated below each rose diagram, whereas the number of the depicted lines are indicated at the top of the rose diagrams. a-c) Central BBHVF, d) Kovácsi-hills Group. (For interpretation of the references to colour in this figure legend, the reader is referred to the web version of this article.)

4.4. Kernel density distribution (heatmap as GIS terminology)

This method enables visualizing the distribution pattern of points (i.e., volcanic centers) in a defined area. 5 km, 7 km, and 10 km search radii were used (Fig. 5a-c) (Appendix A/3). Similar usage of this method is published in Trippanera et al. (2018). All three maps show that the densest area of the BBHVF in the middle part of Central BBHVF, in the vicinity of the Fekete-hegy (Fig. 1b and its corresponding Table 1). The 5 km radius puts this part a few km to the west in contrast to other radii. Another dense area is the Kovácsi-hills Group, where at least 8 eruption centers can be found in short distances (Figs. 1b, 5).

4.5. Orientation of volcanic lineaments

To identify any correlation between regional structural lines and the spatial distribution of volcanoes, it is necessary to examine whether volcanic centers are situated along lines (Connor, 1990; Connor et al., 1992; Valentine and Perry, 2007; Le Corvec et al., 2013c; Tadini et al., 2014; Cañon-Tapia, 2021). All possible vent alignments are considered using lines that connect all vent centers to all others with GIS methods. In this way, it is possible to visualize on a rose diagram the orientation(s) suggested by the lineaments, and possible match with the direction of fault line(s). This kind of method has not been used before. We believe that the largest number of "lines" with at least 3 volcanic centers pointing in the same direction is a good representation of the volcanic lineaments, whose correlation with the structural geological lineaments (faults) is worth investigating. We used 50 m, 200 m, and 500 m tolerance zones (buffers) around lineaments to avoid any inaccuracy caused by the manual marking of volcanic centers. All technical details can be seen in Appendix A/4. The resulting rose diagrams showing the orientation of the volcanic lineaments is shown in Fig. 6. It has to be highlighted that not all the resulting volcanic lineaments can be linked to real geological structures. However, in areas where a large number of volcanic lineaments show the same directions, which are parallel with major faults (Fig. 6), it has to be assumed that they are real volcanic lineaments related to the structural geological environment. This workflow was carried out both on the whole BBHVF, on Central BBHVF and on Kovácsi-hills Group. However, in Kovácsi-hills Group, from the tolerance zones only the 200 m were used because of the short distance between the volcanoes. Using larger tolerance zones could have led to misinterpretation due to the small number of vents.

BBHVF is a NE-SW elongated volcanic field (Fig. 1b), thus, the lines between the points furthest apart are possibly overrepresented (i.e., the NE-SW oriented lines also), because longer lines give more chance to a third point falls into the tolerance zone of each line. To eliminate this uncertainty, we calculated the "center of gravity" (calculated centroid) of the Central BBHVF using the *Mean coordinate* vector analyzing tool, then created a circle around the centroid point with 5, 10, and 15 km radii (in order to exclude the effect of the different radius; Fig. 7). All points (volcanic centers) falling within each zone were selected one after the other (Fig. 7a,b,c). On these three groups of points, the whole workflow was carried out once again.

The rose diagrams clearly show the domination of the NE-SW directed lineaments in case of the Central BBHVF (Fig. 6), which is supplemented by the lineaments of the 5, 10, and 15 km zone around the "center of gravity" of the BBHVF (Fig. 7). There is larger scattering when

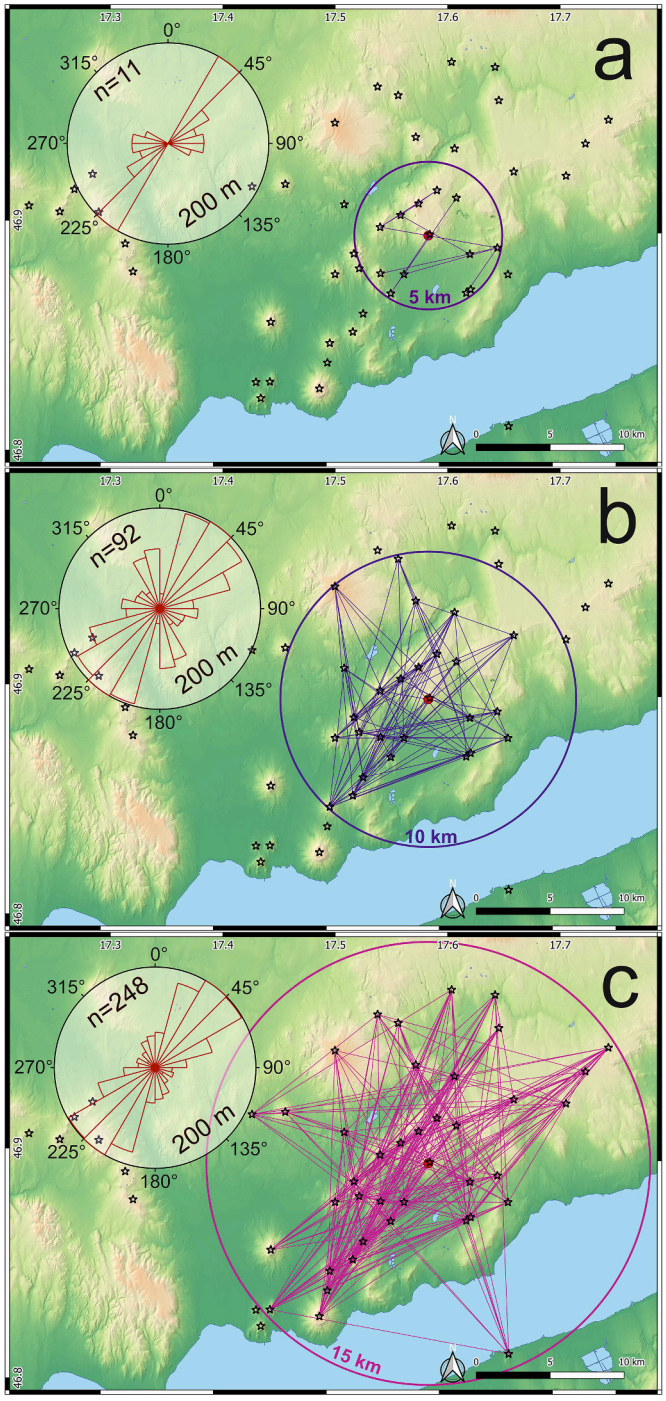

Fig. 7. The maps show the calculated volcanic lineaments (depicted only by using 200 m tolerance zone) in the centrum zone of the Central BBHVF with 5 km (a), 10 km (b), and 15 km (c) radius around it. Red point showing the calculated mean coordinate of the Central BBHVF. Volcanoes inside each circle were used for identifying volcanic lineaments in each case. Rose diagrams showing the orientations of the volcanic lineaments. Legend is identical with Fig. 6. (For interpretation of the references to colour in this figure legend, the reader is referred to the web version of this article.)

larger tolerance zones are used, but also in these cases, the main direction remains NE-SW (ENE-WSW). The main alignments of the Kovácsi-hills Group are WNW-ESE oriented (Fig. 6). There is also a subordinate, NNW-SSE trending volcanic lineament peak in the rose diagrams (Fig. 6d).

4.6. Distance from faults

Distance calculations for each volcanic centers from fault lines (based on Budai et al., 1999b) were carried out (Fig. 8; technical details can be found in Appendix A/5). The cited study presented the last structural geological map about the area. The resulted and visualized lines (Fig. 8) clearly draw two areas, where the volcanoes are sitting on or situated to the northwest in a relatively short distance from the LF, or from an unnamed sinistral strike-slip fault southeast from LF. Based on the inclination of the faults here (Budai et al., 1999a), the zones northwest from the faults (especially in case of LF) are the hanging walls of the fault zones. The lineaments of the studied volcanoes here are the same as that of the orientation of the LF. There are sporadic (<10%) occurrences of volcanoes which are situated not exclusively in the vicinity of these two faults, or >2 km from one. Kovácsi-hills Group is situated in the vicinity of NW-SE striking normal faults, or strike-slip faults.

4.7. Temporal pattern of the volcanism

The technical details are contained in Appendix A/6. The classification resulted in 5 groups; the group number was assigned to the eruption center (based on breaks in the histogram of ages, see Appendix A/6). Thus, the spatial distribution of each group can be analyzed and visualized in a GIS software (Fig. 9a). Oldest volcanic remnants (e.g., Hegyes-tű, Tihany) are situated in the south-eastern part of the BBHVF. These volcanoes are in relatively large distance (>2 km) from the central region of the volcanic field, and from the major fault line (LF) crossing through the BBHVF. It is important to note that 17 volcanic centers have no age data (Table 1; Fig. 9a).

The correlation between the distance from the densest part of the volcanic field and the age of the volcanoes appears to be an intriguing aspect to explore. A medium strength linear correlation was calculated between the distance from the densest part of the volcanic field and the age of each volcanic center ($R^2 = 0.3168$), trendline is shown in Fig. 9b. There is no (or at least weak) correlation between the distance from the LF and the age of the volcanic centers ($R^2 = 0.0201$), trendline is shown in Fig. 9c.

4.8. Magnetic anomaly in the vicinity of volcanic centers

Stalling and crystallizing magma at depths forming subvolcanic bodies (sills, dikes) causing positive or negative anomalies in (aero) magnetic signatures have been mapped for the area (Kiss, 2015). These anomalies are related to the surface extent of the volcanic edifice, but also there is a slight correlation with the size of the subvolcanic bodies (Kiss, 2015). To obtain information about subvolcanic structure of volcanoes, magnetic ΔZ anomaly map was used (https://map.mbfsz.gov.hu/magneses_anomalia/), implemented into the GIS database (Fig. 10). Several studies have been demonstrated that the magnetic anomalies (signatures) provide valuable information on the subvolcanic structures of a volcanic terrain, which are covered by the volcanoes or other non-volcanic formations (e.g., Hildenbrand et al., 1993; Araña et al., 2000; Secomandi et al., 2003; Kiss, 2015).

For the interpretation of the magnetic anomaly map it should be considered that the large positive or negative anomalies not necessarily suggest large crystallized magmatic bodies but can also be the result of the presence of large-volume volcanic edifices nearby (e.g., shield volcanoes, like Kab-hegy, or Agár-tető, Fig. 1b). However, as seen in Fig. 10 there are many areas, where no such high-volume volcanic edifice can be observed. For example, Tihany is characterized by a large roundish positive anomaly right below the maar volcanoes (Németh et al., 2001). Similarly, a positive anomaly can be found under the emblematic butte of Badacsony, which passes under Lake Balaton, and similar can also be seen under Som-hegy, and Halom-hegy volcanoes. This kind of anomaly occurs in the eastern bay of Lake Balaton, where many sill-dyke systems

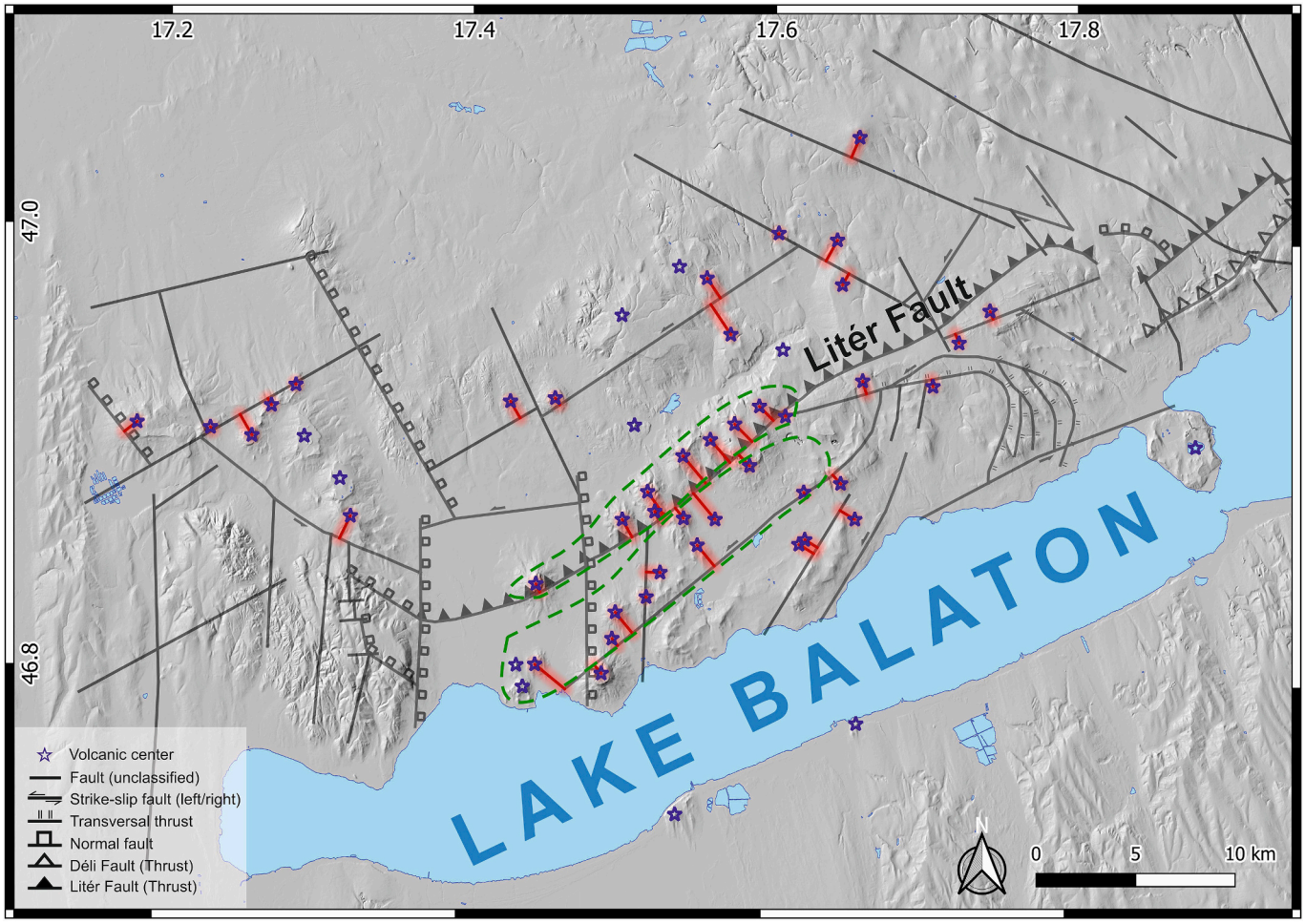

Fig. 8. Distance of faults (Budai et al., 1999b) and volcanic centers. The red lines represent the distance from the fault to the volcanic centers that are located within the 2-km-wide tolerance zone of the faults. Polygons with green dashed line showing two areas where the volcanoes are sitting on or situated to the northwest in a relatively short distance from the Litér Fault (LF), or from an unnamed sinistral strike-slip fault southeast from LF. (For interpretation of the references to colour in this figure legend, the reader is referred to the web version of this article.)

have been inferred (Balázs et al., 2011). The positive magnetic anomaly is significant in the vicinity of the largest volcanic edifices of the BBHVF, such as the shield volcanoes of Agár-tető and Kab-hegy (Fig. 1). In addition to the above, a significant magnetic anomaly can be seen in the Kovácsi-hills Group, where a previous study (Németh and Martin, 2007) documented the surface outcrop of mainly subvolcanic bodies.

5. Discussion

5.1. Differences in the structural geological environment and the volcanic evolution

The shield volcanoes in the BBHVF (Agár-tető and Kab-hegy) differ from the smaller volcanic centers (which are mainly located in the Central BBHVF) not only because of their size and position, but also because of the strong magnetic anomaly in their surroundings. This is possibly caused by 1) more evolved and diverse magmatic system or crystallized subvolcanic basaltic bodies in shallow depth under the shield volcanoes or 2) large volume of basaltic body composing the shield volcanoes themselves. Similar large magnetic anomaly can be observed in the vicinity of Kovácsi-hills Group. This corresponds well with the physical volcanological observations: in this sub-area there are mainly exhumed subvolcanic basaltic bodies, which now form positive landforms due to intense erosion and bedrock heterogeneities (Németh and Martin, 2007). One important reason why this sub-area is different from the Central BBHVF (also in terms of magnetic anomalies) can be the possibly different (faster) erosion rate in the vicinity of Kovácsi-hills Group causing a deeper excavation of the subvolcanic structure of the once-existed maar-diatremes or tuff rings (Németh and Martin, 2007). Another factor can be that melts were rarely able to reach the surface in the case of Kovácsi-hills Group, they stalled at a few hundred meters (~ 200 m) paleodepth (Németh and Martin, 2007). The latter is also a possibility because this sub-area has a different orientation and structural geology (types and striking direction of faults) than the Central BBHVF, so it is possible that the upwelling magma encountered completely different conditions in the upper crust causing different volcanism on the surface (or lack of volcanic eruptions and crystallizing magma under the surface). Overall, Kovácsi-hills Group is characterized by diverse magnetic anomalies, whereas in Central BBHVF magnetic anomalies are sporadic and associated with volcanoes of largest surface volume with some exception.

5.2. Spatial and temporal patterns of volcanism in the vicinity of the Litér Fault

Volcanic lineaments do not necessarily suggest tabular intrusions, nor indicate directly a regional stress direction (Cañon-Tapia, 2021). However, our results demonstrate clear evidence for volcanic lineaments along major upper crustal faults (Figs. 6, 8), implying that major fault zones – as inherited structures – had a significant impact on the

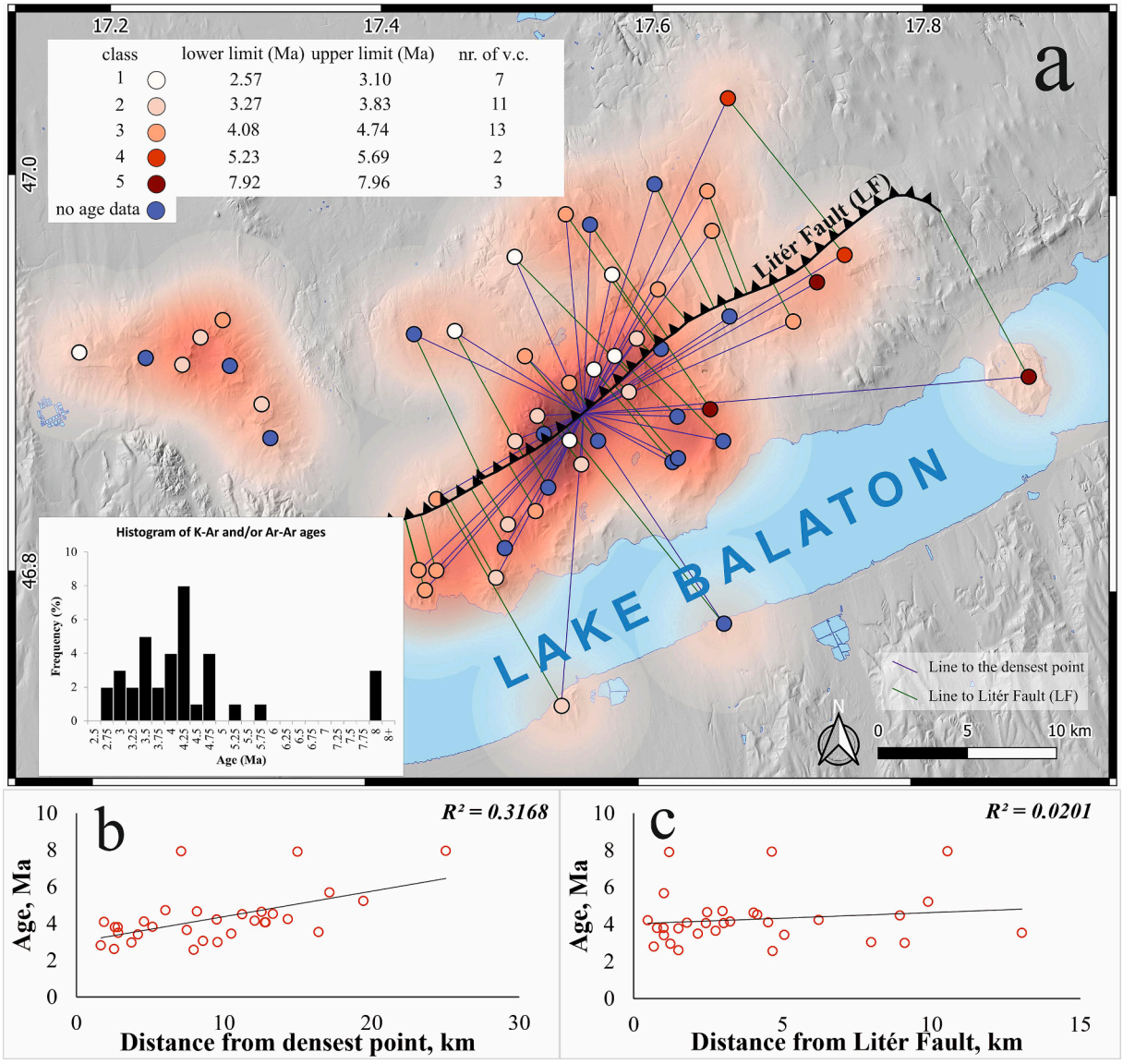

Fig. 9. Location of the various age classes of volcanic centers in the Central BBHVF with respect to the LF. a) Kernel density distribution map was depicted with a 5 km search radius (Fig. 5a) with volcanic centers, which are colored based on the result of the Jenks natural breaks analysis (table in top left corner). Here, age groups or 'classes' were classified for the volcanism of the BBHVF. Histogram (bottom left corner) was created using the available ages with 0.25 Ma bins to present the temporality of the volcanism. The blue lines are created with *Distance to the nearest hub (line to hub)* tool in QGIS® to connect the densest point (which was selected manually) to each volcano. Green lines connect volcanoes to the closest point of the LF (depicted based on Budai et al., 1999b). b) Age versus distance from the densest point plot, which shows a medium strong correlation ($R^2 = 0.3168$). c) Age versus distance from LF plot, which shows weak or no correlation ($R^2 = 0.0201$). Note that only those vents are plotted which have available age data. nr. of v.c.: number of volcanic centers. (For interpretation of the references to colour in this figure legend, the reader is referred to the web version of this article.)

ascending melt and resulted volcanic activity on the surface in terms of spatial distribution. As shown in Fig. 9a-b there is a weak correlation between age and the distance of volcanic centers from the central area of the BBHVF, i.e., volcanoes settled around the core area tend to be younger. It cannot be stated with certainty because of the scarcity of available and reliable age data, but it suggests that there may be such a temporal pattern of the volcanism. A further detailed age measurement campaign would be needed to clarify this issue.

The LF appears to be a key structural element influencing melt ascent and eventually the position of the volcanoes; however, it dips towards the NW (before flattening in the depth of ca. 10 km, Fig. 11) and hence cannot explain volcanic edifices that are located SE from its surface location. Further fault structures have been mapped in this area, which could have played a role in focusing melts as it was demonstrated in case of distance of faults and volcanic centers examination (Fig. 8). These are SW-NE trending Triassic normal faults (Fodor et al., 2020), WSW-ENE trending strike-slip faults that were probably active in the Cretaceous (Budai et al., 1999b; Fodor et al., 2020) and have moderate to minor displacements. Most importantly, a supposed strike-slip fault SE from LF (see Fig. 8, next to the southern green dashed polygon; Budai et al., 1999b) could also have played a role in the transportation of the magmas towards the surface (see an unnamed strike-slip fault SE from LF, Fig. 1b), which is suggested by the alignment of volcanic centers NW from this fault. The volcanic lineament is evidence for channelizing of the melts, however, note that the presence of this strike-slip fault is not confirmed by the latest structural mapping studies (Fodor et al., 2017; Koroknai et al., 2020; Wórum et al., 2020).

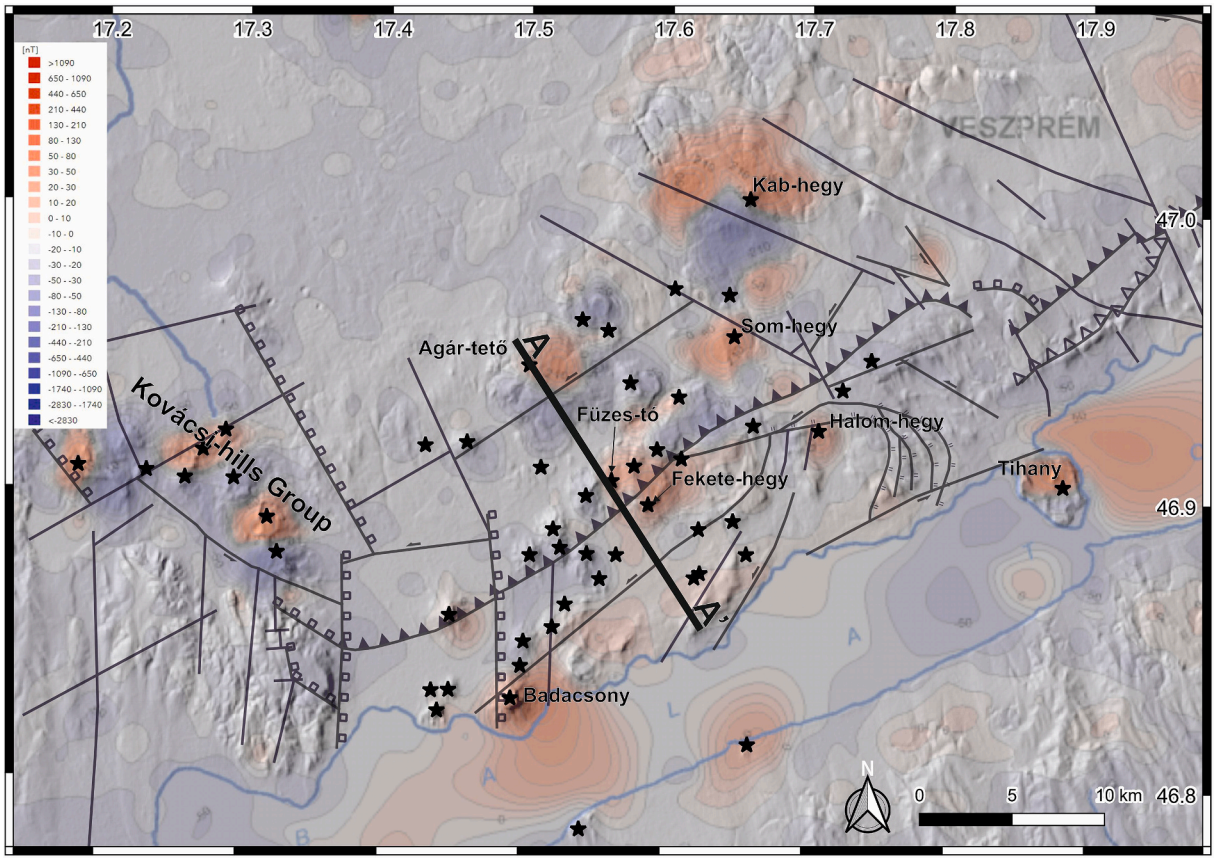

Fig. 10. Magnetic anomaly map of the BBHVF (source: https://map.mbfsz.gov.hu/magneses_anomalia/; Kiss and Gulyás, 2006). Cross section of A-A' is shown in Fig. 11.

5.3. The role of structures and stress field in melt ascent

In the past, many authors stated that volcanism only occurs in extensional or transtensional settings, and in compressional settings, sills should form, thus associated surface volcanism should be rare or absent (Hamilton, 1995; Watanabe et al., 1999). Later, it has been demonstrated, based on detailed field mapping of subvolcanic rocks and experimental studies, that during transpressional tectonic stress period, small volume of melts could successfully reach the surface throughout the lithosphere (Saint Blanquat et al., 1998; Marcotte et al., 2005; Galland et al., 2003, 2007a, 2007b; Norini et al., 2013; Jaldín et al., 2022).

The BBHVF is situated in the Pannonian Basin, which has been under NE-SW compression/transpression and shortening from the late Miocene (Csontos et al., 1992; Fodor et al., 1999) until nowadays (Bada et al., 2007; Békési et al., 2023; Porkoláb et al., 2023), during the whole period of the volcanism (Seghedi et al., 2004). The main faults in the region (e.g., Litér Fault) are oriented roughly NE-SW, therefore they are roughly parallel to the orientation of the maximum principal stress (sigma 1) during the volcanism (Békési et al., 2023). Fractures in the damage zone of faults may open up against the minimal principal stress (sigma 3) in response to fluid pressure increase (Hubbert and Willis, 1957; Gudmundsson, 2011). This means that the opening of fractures in the damage zone of the LF (or other NE-SW trending faults) in response to initial melt transport was possibly aided by the parallel, NE-SW orientation of sigma 1. In case of compressional or transpressional state (sigma 3 is subvertical), subhorizontal fractures may open up, whereas strike-slip stress regimes (sigma 3 is subhorizontal, in our case NW-SE oriented) favor the opening of subvertical, NE-SW trending fractures. Hence, the generally transpressional stress state inferred for the period of volcanism favors the opening of subhorizontal fractures along the deeper, flat section of the LF (Fig. 11) in response to melt injection from below. Therefore, we speculate that this flat, ca. a 10 km deep fault segment could have acted as a "catchment area" for melts across a relatively large, ca. 10 × 30 km area, and focused the melts into fault-parallel channels. We emphasize that the damage zone of such a significant thrust could be suitable for focusing fluid flow, and the possible opening of fractures in response to fluid pressure increase is an additional mechanism that could contribute to this process. Also, in case of temporal stress field changes (e.g., from transpressional to strike-slip), different set of fractures may open subsequently, which could also modify melt transport directions. This would be in line with interpretations that a changing stress field may create the possibility for small-volume melts to reach the surface, such as in the case of the Tilocálar monogenetic volcanic field (Ureta et al., 2021b).

To present the pathway of BBHVF magmas originated in the asthenosphere until the surface, a lithospheric cross-section was created (Fig. 11). In the following paragraph, details are provided from the literature and from current study to see and understand the upwelling of the magma from the source to the surface, which took from hour to days according to recent magma ascent rate estimates (Jankovics et al., 2013). The alkaline basaltic magmas of the BBHVF originated by small degrees partial melting in the asthenosphere (Embey-Isztin et al., 1993; Seghedi et al., 2004; Harangi et al., 2015; Kovács et al., 2020). The exact reasons for the small degrees of partial melting are debated and include the presence of pyroxenitic lithologies, decompression melting and wet asthenosphere. After the asthenospheric melt formation and melt segregation, the pathway of the melts probably was subvertical until the Moho, which may have been facilitated by viscous decompaction processes and the subvertical foliation of the asthenosphere and the coeval compression (Connolly and Podladchikov, 2007; Kovács et al., 2012, 2020; Liptai et al., 2022) with a possible short stall in the vicinity of the Moho. This process may have caused underplating and granulite facies

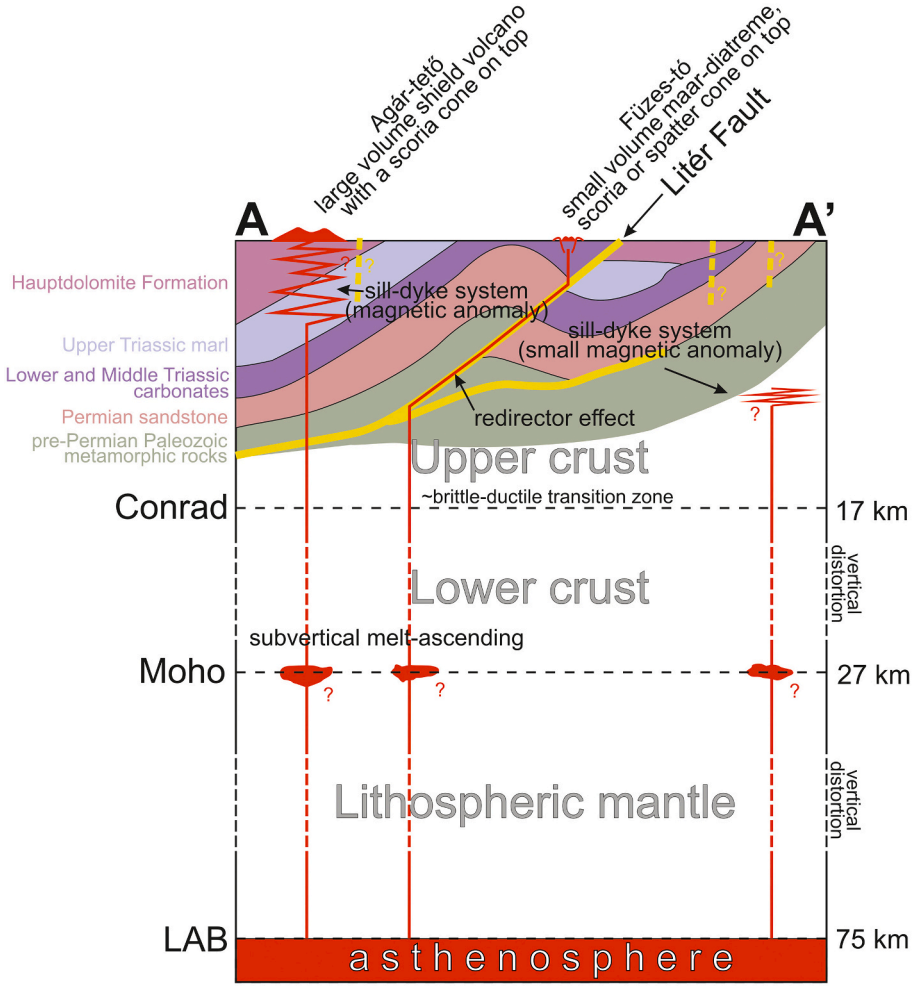

Fig. 11. Schematic and simplified model about the redirector effect of the Litér Fault (LF) in the BBHVF. The position of the cross section can be seen in Fig. 10. Location and dip direction of the faults are based on Budai et al. (1999a) and Fodor et al. (2017). Geologic structure of the upper crust is based on Fodor et al. (2017); however, presence of faults marked with yellow dashed lines is questionable. The stall of the magma in the vicinity of the Moho is suggested by Jankovics et al. (2012). Note, that the asthenospheric source is much more diverse and random than represented here. Conrad discontinuity and Moho (Mohorovičić discontinuity) depths are based on Kalmár et al. (2021), LAB (lithosphere-asthenosphere boundary) depth is based on Kalmár et al. (2023). Horizontal and vertical distances are not comparable. (For interpretation of the references to colour in this figure legend, the reader is referred to the web version of this article.)

metamorphism (Embey-Isztin et al., 1990; Török et al., 2005; Török, 2012) and fractionation of various phenocrysts in the basalts (Jankovics et al., 2012). The fate of the basaltic melt in the ductile lower crust is less clear, but it may well be that subvertical deformation zones are present which facilitate further melt transport to higher levels of the crust (Vauchez et al., 2012; Koptev et al., 2021) The feet of the faults in the brittle upper crust are at least 10 km in depth, which is possibly near the Conrad discontinuity, as well as the lithospheric brittle-ductile transition zone (Fig. 11). This depth also seems to coincide with the usual depths of earthquakes in the Pannonian Basin (Wéber, 2018) and with the approximate depth of the well conductive zone beneath the BBHVF (e.g., Ádám et al., 2017) presumably marking an important boundary in terms of rheology and structural geology (i.e., subhorizontal Alpine nappe boundary; Tari and Horváth, 2010). Thus, it is likely when magma reached the rheologically brittle deformation zone, fault planes as weakness zones in the crust could play a role in transporting the melt towards the surface. Experimental studies show that the emplacement of volcanoes in case of horizontal crustal shortening environment will take place: 1) at the intersection between the fault plane and the *syn*-volcanic surface; or 2) ascend temporarily along the fault plane, then migrate vertically if the buoyancy enable to break through the basement rocks (Tibaldi et al., 2009). This process results in a spatially clustered volcano distribution along LF, and not on the fault plane-surface intersection, but on the hanging wall. This statement does not suggest necessarily that the source melting extent was identical to the surface patterns of volcanoes. Instead, melt pathways are most probably controlled by local heterogeneities of the ductile lithosphere layers, and then the melt is channelized by major upper crustal faults leading the magmas to reach the surface close to the surface-fault intersection (Fig. 11). Based on our results, we interpret the BBHVF as an example of the above-described magma transport model, where major upper crustal inherited structures most probably focused the ascent of melts causing clustered distribution of volcanic centers, volcanic lineaments in most cases with the same orientation as the main inactive reverse fault (LF). Strike-slip faults located SE from the LF might also have contributed to the focusing (according to a second group of volcanic centers clustered along a line SE from LF; Fig. 8), as strike-slip faults in general favor upwelling of the magma (Tibaldi et al., 2009). Results show that some volcanoes also formed independently of this main fault zone (e.g., Agár-tető, Kab-hegy). There is also a difference in the volcanic landform: Kab-hegy and Agár-tető (Fig. 1b) are shield volcanoes dominated by prolonged (few 100 ky active period) effusive or at most Strombolian explosive activity, whereas other volcanoes of the Central BBHVF (Fig. 1b) were maar-diatremes formed via phreatomagmatic explosive eruptions fed by small-volume of magma (Martin et al., 2003; Kereszturi et al., 2011). The longer active period of these shield volcanoes suggests stable

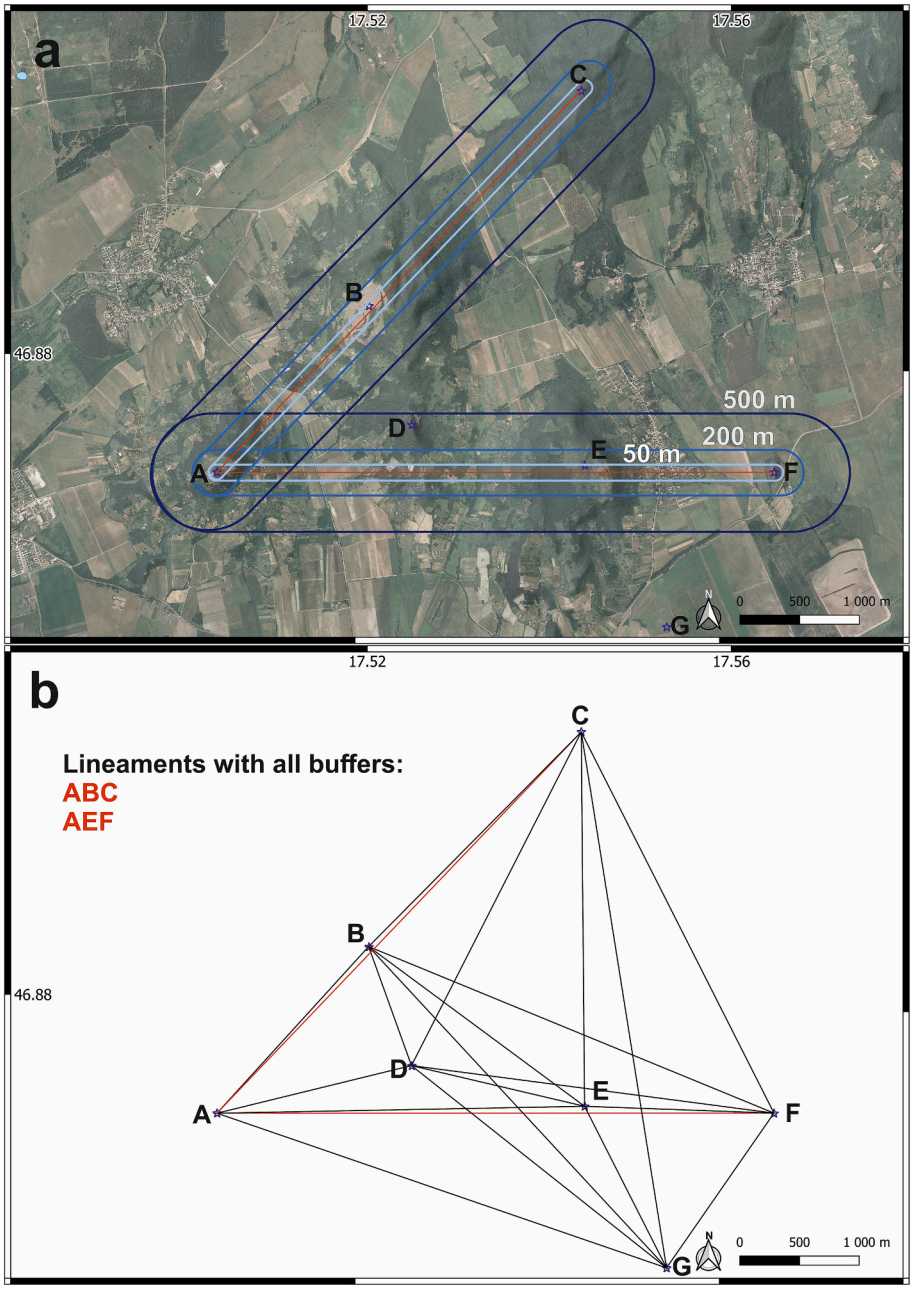

Fig. 12. An example from a smaller area of the BBHVF to the created tolerance zones (a), and all possible point pairs connected with lines of the same area (b). Note that in case of A-F and A-C lines using all tolerance zones will result in lineaments containing points of ABC and AEF. Satellite imagery is from Google.

magmatic system, and indicates that buoyancy forces alone may also be enough for the melt to make its way to the surface even across the brittle upper crust independently from major crustal weakness zones (Fig. 11). Buoyancy-driven ascent resulted in a longer active period for these volcanoes with several eruptions, and significant volume (Kereszturi et al., 2011) in contrast to other volcanoes in the BBHVF in the vicinity of the LF, or the strike-slip fault SE from it (see Fig. 1b; Kereszturi et al., 2011).

These results highlight the importance of field-based structural geological investigations supplemented by wide GIS analyses in active monogenetic volcanic fields. The clustering coming from the channelizing effect of major faults should also be taken into account when assessing volcanic hazards in active volcanic fields (e.g., Magill et al., 2005; Kereszturi et al., 2014; Sieron et al., 2021). In case of BBHVF, from a regional geological point of view, extensive dating is necessary to date the volcanic cycles more accurately, to understand the structure of the lithosphere and the role of the lithospheric weaknesses throughout the volcanic evolution of the BBHVF.

6. Conclusion

In this study spatial and temporal patterns of the monogenetic volcanoes of the Mio-Pleistocene Bakony-Balaton Highland Volcanic Field situated in a compressional/transpressional tectonic regime in back-arc setting were studied. The main results are summarized as follows:

1) GIS methodology provides a useful toolkit to investigate the contribution of lithospheric properties and volcanism of a defined area. All used tools and modules are freeware and/or open-source, results can be reproduced freely. All software is available publicly and can be used even in regions where resources to access software are limited,

and the workflow and perspective can be easily adapted to other volcanic areas.

2) The BBHVF can be separated into two sub-areas. The main types of volcanic remnants are different in the two sub-areas (maar-diatremes vs. subvolcanic magmatic bodies). The distribution of the volcanic centers is statistically proven not random, but clustered.
3) The orientations of the two sub-areas within the BBHVF align closely with the orientations of major fault systems. This observation suggests that the locations of volcanoes are likely influenced by the underlying tectonic framework (i.e., are tectonically determined). Volcanic lineaments, which follow fault geometries, provide further evidence of this tectonic control.
4) Density of the volcanic center distribution is the largest in the central area of the BBHVF along an inactive thrust fault (Litér Fault). Based on our results, this fault emerges as a key structural element influencing melt ascent and the positioning of volcanoes. We speculate that the NW dipping fault plane of Litér Fault could be a 'catchment area' in the upper crust, which channelized the magmas and helped them reach the surface. Larger shield volcanoes situated in larger distance from the Litér Fault have typically longer active period (several 100 ky), thus their magmatic system could be stable, and buoyancy of the magma was enough to bring the basaltic melt to the surface without the help of any fault planes causing long-lasting effusive and small explosive activity.
5) This study underscores the significance of structural geological investigations in monogenetic volcanic fields supplemented by multiple GIS tools. The clustering of volcanic centers along major inherited structures should be considered when assessing volcanic hazards.

CRediT authorship contribution statement

Mátyás Hencz: Conceptualization, Methodology, Investigation, Writing – original draft. **Tamás Biró:** Conceptualization, Methodology, Investigation, Software, Writing – review & editing. **Károly Németh:** Conceptualization, Methodology, Supervision, Writing – review & editing. **Kristóf Porkoláb:** Writing – review & editing. **István János Kovács:** Writing – review & editing. **Tamás Spránitz:** Writing – review & editing. **Sierd Cloetingh:** Conceptualization, Writing – review & editing. **Csaba Szabó:** Conceptualization, Supervision, Writing – review & editing. **Márta Berkesi:** Conceptualization, Supervision, Writing – review & editing.

Declaration of Competing Interest

The authors declare the following financial interests/personal relationships which may be considered as potential competing interests:

Mátyás Hencz reports financial support was provided by Hungarian Academy of Sciences. Márta Berkesi reports financial support was provided by Hungarian Academy of Sciences. Tamás Spránitz reports financial support was provided by Hungarian Academy of Sciences. István János Kovács reports financial support was provided by Hungarian Academy of Sciences.

Data availability

No data was used for the research described in the article.

Acknowledgements

The work was financed by the MTA FI FluidsByDepth Lendület (Momentum) project, provided by the Hungarian Academy of Sciences (grant nr. LP2022-2/2022). The focus of our research group (MTA FI FluidsByDepth Lendület Research Group) is to understand the movements of the fluids (especially the CO_2) in the lithosphere from the mantle to the surface, and the sample area is the BBHVF. The study was also partially financed by the MTA FI Pannon LitH_2Oscope Lendület (Momentum) project, provided by the Hungarian Academy of Sciences (grant nr. LP2018-5/2022). Sierd Cloetingh was supported by the Distinguished Guest Scientist Fellowship Program of the Hungarian Academy of Sciences. The authors are grateful to Dániel Kalmár, Thomas Lange and Eszter Békési for the fruitful discussions, which helped to improve the manuscript. The Hydrodem hydrologically improved digital elevation model (which was used as the base layer for our maps) was provided by the Lechner Tudásközpont Nonprofit Kft. We are grateful to Gianluca Norini, Gianluca Groppelli and an anonymous reviewer for in-depth constructive reviews. This is publication no. 124. of the Lithosphere Fluid Research Lab.

Appendix A. Methods in details

A.1. Nearest neighbor (NN) analysis

Based on the methodology described by Le Corvec et al. (2013c) and Uslular et al. (2021) the Geological Image Analysis Software optimized to MATLAB® (GIAS, Beggan and Hamilton, 2010) was used to statistically quantify clustering of volcanic vents in the BBHVF. Output file of the GIAS containing all statistical results can be found as Supplementary Material 1.

A.2. Orientation of the volcanic field compared to the main faults

Bounding polygon geometry of Minimum bounding geometry algorithm in QGIS® was used for each subset of eruption centers. It was possible to create a rose diagram for the orientation of longer sides of the polygons using the Line Direction Histogram module of QGIS®. The rose diagram can be seen in Fig. 4a. The same module was used to visualize the orientation of the fault lines within the BBHVF and its vicinity (the used faults are shown in Fig. 4 as white solid lines).

A.3. Kernel density distribution

Heatmap (Kernel Density Estimation) function of the QGIS® was used to visualize the density of the volcanic centers' distribution (Fig. 5).

A.4. Orientation of volcanic lineaments

Thus, recent studies used several methods to identify volcanic lineaments and draw conclusions for the relationship of pre-existing fractures and locations of volcanism (e.g., Valentine and Perry, 2007; Tadini et al., 2014). Volcanic alignments or lineaments mean the recognition groups of points (at least three) in space (where points refer to volcanoes or vents), which lie in a straight line in space considering a tolerance zone around the line (Connor et al., 1992, 2000; von Veh and Németh, 2009; Le Corvec et al., 2013c). In contrast to Le Corvec et al. (2013c), length tolerance was not applied. Every possible connecting line between volcanoes was used, but separately for the two delimited areas (Central BBHVF, Kovácsi-hills Group). The tolerance zone and longevity of the straight line depend on the size of the investigated volcanic field and the number and spatial density of volcanic vents. At first, to all volcanic centers' coordinates, the coordinates of all other vents were attributed with filtering the duplicate pairs (e.g., A-B is the same as B-A, thus B-A is filtered out). This step was carried out by applying Python's enumerate and list comprehension on a list containing x and y coordinates of all volcanoes. Then, all pairs were treated as endpoints of sections, thus lines were drawn between endpoints using the XY to Line function of QGIS® module Shape Tools. A tolerance (buffer) zone was created for each line using the Buffer geoprocessing tool with three different distances: 50 m, 200 m, 500 m. An example from a smaller area can be seen in Fig. 12. Then the included points (volcanic centers) of each tolerance zone (can be handled as polygons) was counted using Count Points in Polygon vector analysis tool. The zones containing <3

points (volcanic centers) were filtered out, because the minimal number of points for creating a lineament is 3 (Le Corvec et al., 2013c). The remaining polygons were reconverted to lines. Then, orientation of these lines was visualized using the Line Direction Histogram module of QGIS®.

This workflow was carried out both on the whole BBHVF, on Central BBHVF and on Kovácsi-hills Group; however, in case of Kovácsi-hills Group, from the tolerance zones only the 200 m were used because of the short distance between the volcanoes. Using larger tolerance zones could have led to misinterpretation due to the small number of volcanic centers.

A.5. Distance from faults

Faults of Budai et al. (1999b) were converted to points in 1 m distance from each other using Convert lines to points SAGA® tool of QGIS®. Then, with Distance to the nearest hub (line to hub) tool, lines to the nearest point of the faults were calculated. Fig. 8. shows the lines with red to the closest point of the nearest fault if the distance is <2 km.

A.6. Temporal pattern of the volcanism

A histogram of the ages was created using 0.25 Ma bins, where visually at least 5 higher columns, i.e., larger breaks in the numerical series of the ages are visible (Fig. 9). Histogram suggests a younger and an older group in the period from 2.57 Ma to 3.83 Ma (see Fig. 9), which is dedicated as the younger volcanic period of the BBHVF. In all other cases, at least 200,000 years have passed between two groups. A histogram of the ages was created using 0.25 Ma bins, where visually at least 5 higher columns, i.e., larger breaks in the numerical series of the ages are visible (Fig. 9). Thus, the data was split into 5 classes in order to minimize the squared deviation within each class. This task was carried out with Jenks Natural Breaks function of Xrealstats free Microsoft Excel® plugin (see detailed description: https://real-statistics.com) with the number of 5 classes (4 natural breaks). Jenks natural break method reduces the variance within classes, while maximizing the variance between classes (Jenks, 1967).

The centrum of the densest part (darkest red in Fig. 5b) was selected manually. Then, with Distance to the nearest hub (line to hub) tool in QGIS®, lines (Fig. 9a) and their lengths (Supplementary Material 2) to the centrum of the densest part from each volcano were calculated. Only volcano-centrum length data were used where age data was available for the volcano. Then, LF (based on Budai et al., 1999b) was transformed into points with Convert lines to points SAGA® tool of QGIS®. Then, with Distance to the nearest hub (line to hub) tool, lines from the vents to the nearest point of the LF were calculated (Supplementary Material 2).

Appendix B. Supplementary data

Supplementary data to this article can be found online at https://doi.org/10.1016/j.jvolgeores.2023.107940.

References

Ádám, A., Szarka, L., Novák, A., Wesztergom, V., 2017. Key results on deep electrical conductivity anomalies in the Pannonian Basin (PB), and their geodynamic aspects. Acta Geodaet. Geophys. 52, 205–228. https://doi.org/10.1007/s40328-016-0192-2.

Araña, V., Camacho, A.G., Gracia, A., Montesinos, F.G., Blanco, I., Vieira, R., Felpeto, A., 2000. Internal structure of Tenerife (Canary Islands) based on gravity, aeromagnetic and volcanological data. J. Volcanol. Geotherm. Res. 103 (1–4), 43–64. https://doi.org/10.1016/S0377-0273(00)00215-8.

Bada, G., Horváth, F., Dövényi, P., Szafián, P., Windhoffer, G., Cloething, S., 2007. Present-day stress field and tectonic inversion in the Pannonian basin. Glob. Planet. Chang. 58 (1–4), 165–180. https://doi.org/10.1016/j.gloplacha.2007.01.007.

Balázs, A., Király, Á., Bőgér, Á., 2011. Basalt Volcanoes under the Lake Balaton. In: 6th Congress of the Balkan Geophysical Society. European Association of Geoscientists and Engineers. https://doi.org/10.3997/2214-4609-pdb.262.C17.

Balázs, A., Matenco, L., Magyar, I., Horváth, F., Cloetingh, S.A.P.L., 2016. The link between tectonics and sedimentation in back-arc basins: New genetic constraints from the analysis of the Pannonian Basin. Tectonics 36 (6), 1526–1559. https://doi.org/10.1002/2015TC004109.

Balogh, K., Németh, K., 2005. Evidence for the Neogene small-volume intracontinental volcanism in the Western Hungary: K/Ar geochronology of the Tihany Maar Volcanic complex. Geol. Carpath. 56 (1), 91–99.

Balogh, K., Pécskay, Z., 2001. K/Ar and Ar/Ar geochronological studies in the Pannonian–Carpathians–Dinarides (PANCARDI) region. Acta Geol. Hung. 44 (2–3), 281–299.

Balogh, K., Jámbor, Á., Partényi, Z., Ravaszné Baranyai, L., Solti, G., 1982. Radiometric K/Ar age of the transdanubian basalts. Ann. Rep. Hungarian Geol. Inst. 1980, 243–259.

Balogh, K., Árva-Sós, E., Pécskay, Z., Ravasz-Baranyai, L., 1986. K/Ar dating of post-sarmatian alkali basaltic rocks in Hungary. Acta Mineral. Petrograph. 27, 75–93.

Beggan, C., Hamilton, C.W., 2010. New image processing software for analyzing object size-frequency distributions, geometry, orientation, and spatial distribution. Comput. Geosci. 36, 539–549. https://doi.org/10.1016/j.cageo.2009.09.003.

Békési, E., Porkolób, K., Wesztergom, V., Wéber, Z., 2023. Updated stress dataset of the Circum-Pannonian region: implications for regional tectonics and geo-energy applications. Tectonophysics 865, 229860. https://doi.org/10.1016/j.tecto.2023.229860.

Borsy, Z., Balogh, K., Kozák, M., Pécskay, Z., 1987. Újabb adatok a Tapolcai-medence fejlődéstörténetéhez. Közlemények a Debreceni Kossuth Lajos Tudományegyetem Földrajzi Intézetéből 23, 79–104 (in Hungarian).

Brenna, M., Cronin, S.J., Németh, K., Smith, I.E.M., Sohn, Y.K., 2011. The influence of magma plumping complexity on monogenetic eruptions, Jeju Island, Korea. Terra Nova 23, 70–75. https://doi.org/10.1111/j.1365-3121.2010.00985.x.

Budai, T., Császár, G., Csillag, G., Dudko, A., Koloszár, L., Majoros, Gy, 1999a. A Balaton-felvidék földtana. Occasional Papers of the Geological Institute of Hungary, Budapest, p. 197 (in Hungarian).

Budai, T., Császár, G., Csillag, G., Dudko, A., Koloszár, L., Majoros, Gy, 1999b. A Balaton-felvidék földtana – Magyarázó a Balaton-felvidék földtani térképéhez, 1:50 000. In: Vol. 197 of the Occasional Papers of the Geological Institute of Hungary, p. 257 (in Hungarian).

Cañon-Tapia, E., 2021. Vent distribution and sub-volcanic systems: Myths, fallacies, and some plausible facts. Earth Sci. Rev. 221, 103768 https://doi.org/10.1016/j.earscirev.2021.103768.

Clark, P.J., Evans, F.C., 1954. Distance to nearest neighbor as a measure of spatial relationships in populations. Ecology 35, 445–453.

Cloetingh, S., van Wees, J.D., Ziegler, P.A., Lenkey, L., Beekman, F., Tesauro, M., Förster, A., Norden, B., Kaban, M., Hardebol, N., Bonté, D., Genter, A., Guillou-Frottier, L., Ter Voorde, M., Sokoutis, D., Willingshofer, E., Cornu, T., Worum, G., 2010. Lithosphere tectonics and thermo-mechanical properties: an integrated modelling approach for Enhanced Geothermal Systems exploration in Europe. Earth Sci. Rev. 102, 159–206. https://doi.org/10.1016/j.earscirev.2010.05.003.

Connolly, J.A.D., Podladchikov, Y.Y., 2007. Decompaction weakening and channeling instability in ductile porous media: Implications for asthenospheric melt segregation. J. Geophys. Res. 112, B110205. https://doi.org/10.1029/2005JB004213.

Connor, C.B., 1990. Cinder cone clustering in the TransMexican Volcanic Belt: implications for structural and petrologic models. J. Geophys. Res. 95, B12. https://doi.org/10.1029/JB095iB12p19395.

Connor, C.B., Condit, C.D., Crumpler, L.S., Aubele, J.C., 1992. Evidence of regional structural controls on vent distribution: Springerville Volcanic Field, Arizona. J. Geophys. Res. 97 https://doi.org/10.1029/92JB00929.

Connor, C.B., Stamatakos, J.A., Ferrill, D.A., Hill, B.E., Ofoegbu, G.I., Conway, F.M., Sagar, B., Trapp, J., 2000. Geologic factors controlling patterns of small-volume basaltic volcanism: application to a volcanic hazards assessment at Yucca Mountain, Nevada. J. Geophys. Res. 105 (1), 417–432. https://doi.org/10.1029/1999JB900353.

Cook, C., Briggs, R.M., Smith, I.E.M., Maas, R., 2005. Petrology and geochemistry of intraplate basalts in the South Auckland Volcanic Field, New Zealand: evidence for two coeval magma suites from distinct sources. J. Petrol. 4, 473–503. https://doi.org/10.1093/petrology/egh084.

Corazzato, C., Tibaldi, A., 2006. Fracture control on type, morphology and distribution of parasitic volcanic cones: an example from Mt. Etna, Italy. J. Volcanol. Geotherm. Res. 158, 177–194. https://doi.org/10.1016/j.jvolgeores.2006.04.018.

Csicsek, L.Á., Fodor, L., 2016. Imbrication of Middle Triassic rocks near Öskü (Bakony Hills, Western Hungary). Földtani Közlöny 146 (4), 355–370 (in Hungarian with English abstract).

Csontos, L., Nagymarosi, A., Horváth, F., Kovač, M., 1992. Tertiary evolution of the Intra-Carpathian area: a model. Tectonophysics 208 (1–3), 221–241. https://doi.org/10.1016/0040-1951(92)90346-8.

Csorba, P., 2021. Magyarország kistájai. Meridián Táj- és Környezetföldrajzi Alapítvány. Debrecen, p. 409 (in Hungarian).

D'Orazio, M., Agostini, S., Mazzarini, F., Innocenti, F., Manetti, P., Haller, M.J., Lahsen, A., 2000. The Pali Aike Volcanic Field, Patagonia: slab-window magmatism near the tip of South America. Tectonophysics 321, 407–427. https://doi.org/10.1016/S0040-1951(00)00082-2.

Embey-Isztin, A., Scharbert, H.G., Dietrich, H., Poultidis, H., 1990. Mafic granulites and clinopyroxenite xenoliths from the Transdanubian Volcanic Region (Hungary): implications for the deep structure of the Pannonian Basin. Mineral. Mag. 54 (376), 463–483. https://doi.org/10.1180/minmag.1990.054.376.12.

Embey-Isztin, A., Downes, H., James, D.E., Upton, B.G.J., Dobosi, G., Ingram, G.A., Harmon, R.S., Scharbert, H.G., 1993. The petrogenesis of Pliocene alkaline volcanic

rocks from the Pannonian Basin, Eastern Central Europe. J. Petrol. 34 (2), 317–343. https://doi.org/10.1093/petrology/34.2.317.
Fodor, L., Csontos, L., Bada, G., Győrfi, I., Benkovics, L., 1999. Tertiary tectonic evolution of the Pannonian Basin system and neighbouring orogens: a new synthesis of paleostress data. Geol. Soc. Lond. Spec. Publ. 156 (1), 295–334. https://doi.org/10.1144/GSL.SP.1999.156.01.15.
Fodor, L., Héja, G., Kövér, Sz., Csillag, G., Csicsek, L.Á., 2017. Cretaceous deformation of the south-eastern Transdanubian Range Unit, and the effect of inherited Triassic–Jurassic normal faults. Pre-conference Excursion Guide. In: Pál-Molnár, E. (Ed.), 15th Meeting of the Central European Tectonic Studies Group (CETeG), pp. 47–76.
Fodor, L., Héja, G., Kövér, Sz, 2020. Structural geology of the Balaton Highlands and its surroundings. In: Babinszki, E., Horváth, F. (Eds.), Investigating Lake Balaton in the Footsteps of Lajos Lóczy. Magyarhoni Földtani Társulat, Budapest, pp. 73–89.
Fodor, L., Csillag, G., Németh, K., Sebe, K., Telbisz, T., Váradi, K., Visnovitz, F., Balázs, A., 2022. Structural geological interpretation of late Miocene-Pliocene basalt volcanoes and associated morphological surfaces - a new step in the neotectonic analysis of the Transdanubian Mountain Range. In: Fehér, B., Lukács, R., Czuppon, Gy, Kereskényi, E. (Eds.), Calce et malleo – Mésszel és kalapáccsal. 12. Kőzettani és Geokémiai Vándorgyűlés. CSFK Földtani és Geokémiai Intézet, Budapest, pp. 41–43.
Gaffney, E.S., Damjanac, B., Valentine, G.A., 2007. Localization of volcanic activity: 2. Effects of pre-existing structure. Earth Planet. Sci. Lett. 263 (3–4), 323–338. https://doi.org/10.1016/j.epsl.2007.09.002.
Galland, O., de Bremond d'Ars, J., Cobbold, P.R., Hallot, E., 2003. Physical models of magmatic intrusion during thrusting. Terra Nova. https://doi.org/10.1046/j.1365-3121.2003.00512.x.
Galland, O., Cobbold, P.R., de Bremond d'Ars, J., Hallot, E., 2007a. Rise and emplacement of magma during horizontal shortening of the brittle crust: Insights from experimental modelling. J. Geophys. Res. 112, B06402. https://doi.org/10.1029/2006JB004604.
Galland, O., Hallot, E., Cobbold, P.R., Ruffet, G., de Bremod d'Ars, J., 2007b. Volcanism in a compressional Andean setting: a structural and geochronological study of Tromen volcano (Neuquen province, Argentina). Tectonics 26, TC4010. https://doi.org/10.1029/2006TC002011.
Glazner, A.F., Bartley, J.M., 1994. Eruption of alkali basalts during crustal shortening in southern California. Tectonics 13, 493–498. https://doi.org/10.1029/93TC03491.
Gudmundsson, A., 2011. Rock Fractures in Geological Processes. Cambridge University Press. https://doi.org/10.1017/cbo9780511975684.
Gyalog, L., Síkhegyi, F., 2005. Geological Map of Hungary, 1:100.000. Geological Institute of Hungary, Budapest.
Hamilton, W.B., 1995. Subduction systems and magmatism. In: Smellie JR (Ed.) Volcanism Associated with Extension to Consuming Plate margins. Geol. Soc. Lond. Spec. Publ. 81, 3–28. https://doi.org/10.1144/GSL.SP.1994.081.01.02.
Harangi, Sz, Jankovics, É.M., Sági, T., Kiss, B., Lukács, R., Soós, I., 2015. Origin and geodynamic relationships of the late Miocene to Quaternary alkaline basalt volcanism in the Pannonian basin, eastern-Central Europe. Int. J. Earth Sci. 104, 2007–2032. https://doi.org/10.1007/s00531-014-1105-7.
Hencz, M., Karátson, D., Németh, K., Biró, T., 2017. The phreatomagmatic pyroclastic sequence of the Badacsony Hill: implications for the processes and landforms of monogenetic basaltic volcanism. Földtani Közlöny 147 (3), 297–310. https://doi.org/10.23928/foldt.kozl.2017.147.3.297. https://scholar.google.com/citations?view_op=view_citation&hl=hu&user=HZY4JQwAAAAJ&citation_for_view=HZY4JQwAAAAJ:u5HHmVD_uO8C (in Hungarian with English abstract).
Hildenbrand, T.G., Rosenbaum, J.G., Kauahikaua, J.P., 1993. Aeromagnetic study of the island of Hawaii. J. Geophys. Res. Solid Earth 98, 4099–4119. https://doi.org/10.1029/92JB02483.
Horváth, F., Cloetingh, S., 1996. Stress-induced late-stage subsidence anomalies in the Pannonian basin. Tectonophysics 266 (1–4), 287–300. https://doi.org/10.1016/S0040-1951(96)00194-1.
Hubbert, M.K., Willis, D.G., 1957. Mechanics of hydraulic fracturing. Trans. AIME 210 (01), 153–168.
Hughes, S.S., Wetmore, P.H., Casper, J.L., 2002. Evolution of Quaternary tholeiitic basalt eruptive centers on the eastern Snake River Plain, Idaho. In: Bonnichsen, B., White, C.M., McCurry, M. (Eds.), Tectonic and Magmatic Evolution of the Snake River Plain Volcanic Province, 30. Idaho Geological Survey Bulletin, pp. 363–385.
Jaldín, D., Tibaldi, A., Bonali, F.L., Giambiagi, L., Espinoza, D., Luengo, K., Santander, A., Russo, E., 2022. Compressional tectonics and volcanism: the Miocene-Quaternary evolution of the Western Cordillera (24–26°S), Central Andes. Bull. Volcanol. 85, 8. https://doi.org/10.1007/s00445-022-01615-y.
Jankovics, É.M., Harangi, Sz, Kiss, B., Ntaflos, T., 2012. Open-system evolution of the Füzes-tó alkaline basaltic magma, western Pannonian Basin: Constraints from mineral textures and compositions. Lithos 140-141, 25–37. https://doi.org/10.1016/j.lithos.2012.01.020.
Jankovics, É.M., Dobosi, G., Embey-Isztin, A., Kiss, B., Sági, T., Harangi, Sz, Ntaflos, T., 2013. Origin and ascent history of unusually crystal-rich alkaline basaltic magmas from the western Pannonian Basin. Bull. Volcanol. 75, 749. https://doi.org/10.1007/s00445-013-0749-7.
Jankovics, É.M., Harangi, Sz, Németh, K., Kiss, B., Ntaflos, T., 2015. A complex magmatic system beneath the Kissomlyó monogenetic volcano (western Pannonian Basin): evidence from mineral textures, zoning and chemistry. J. Volcanol. Geotherm. Res. 301, 38–55. https://doi.org/10.1016/j.jvolgeores.2015.04.010.
Jenks, G.F., 1967. The data model concept in statistical mapping. Int. Yearbook Cartography 7, 186–190.
Jugovics, L., 1968. A dunántúli bazalt és bazalttufa területek. Ann. Rep. Hungarian Geol. Inst. 1967, 75–82 (in Hungarian).
Kalmár, D., Hetényi, gy., Balázs, A., Bondár, I., AlpArray Working Group, 2021. Crustal thinning from orogen to back-arc basin: the structure of the Pannonian Basin region revealed by P-to-S converted seismic waves. J. Geophys. Res. Solid Earth 126, e2020JB021309. https://doi.org/10.1029/2020JB021309.
Kalmár, D., Petrescu, L., Stipčević, J., Balázs, A., Kovács, I.J., the AlpArray and PACASE Working Groups, 2023. Lithospheric structure of the circum-Pannonian region imaged by S-to-P receiver functions. Geochem. Geophys. Geosyst. 24, e2023GC010937 https://doi.org/10.1029/2023GC010937.
Kereszturi, G., Németh, K., 2012. Monogenetic basaltic volcanoes: genetic classification, growth, geomorphology and degradation. In: Németh, K. (Ed.), Updates in Volcanology – New Advances in Understanding Volcanic Systems. InTech, pp. 3–89. https://doi.org/10.5772/51387.
Kereszturi, G., Németh, K., Csillag, G., Balogh, K., Kovács, J., 2011. The role of external environmental factors in changing eruption styles of monogenetic volcanoes in a Mio/Pleistocene continental volcanic field in western Hungary. J. Volcanol. Geotherm. Res. 201 (1–4), 227–240. https://doi.org/10.1016/j.jvolgeores.2010.08.018.
Kereszturi, G., Geyer, A., Martí, J., Németh, K., Dóniz-Páez, F.J., 2013. Evaluation of morphometry-based dating of monogenetic volcanoes – a case study from Bandas del Sur, Tenerife (Canary Islands). Bull. Volcanol. 75, 734. https://doi.org/10.1007/s00445-013-0734-1.
Kereszturi, G., Németh, K., Cronin, S.J., Procter, J., Agustín-Flores, J., 2014. Influences on the variability of eruption sequences and style transitions in the Auckland Volcanic Field, New Zealand. J. Volcanol. Geotherm. Res. 286, 101–115. https://doi.org/10.1016/j.jvolgeores.2014.09.002.
Kiss, J., 2015. Connection between geomagnetic anomalies and mafic geological formations penetrated by wells in the Pannonian Basin. Magyar Geofizika 56 (1), 21–42 (in Hungarian with English abstract).
Kiss, J., Gulyás, Á., 2006. Magnetic ΔZ Anomaly Map of Hungary, 1: 500.000, Printed Map. Eötvös Loránd Geophysical Institute, Budapest, Hungary.
Kiyosugi, K., Connor, C.B., Zhao, D., Connor, L.J., Tanaka, K., 2010. Relationships between volcano distribution, crustal structure, and P-wave tomography: an example from the Abu Monogenetic Volcano Group, SW Japan. Bull. Volcanol. 72, 331–340. https://doi.org/10.1007/s11004-005-1556-2.
Kiyosugi, K., Conor, C.B., Wetmore, P.H., Ferwerda, B.P., Germa, A.M., Connor, L.J., Hintz, A.R., 2012. Relationship between dike and volcanic conduit distribution in a highly eroded monogenetic volcanic field: San Rafael, Utah, USA. Geology 40, 695–698. https://doi.org/10.1130/G33074.1.
Kókay, J., 1976. Geomechanical investigation of the southeastern margin of the Bakony Mountains and the age of the LF line. Acta Geol. Hung. 20 (3–4), 245–257.
Koptev, A., Cloetingh, S., Kovács, I.J., Gerya, T., Ehlers, T.A., 2021. Controls by rheological structure of the lithosphere on the temporal evolution of continental magmatism: Inferences from the Pannonian Basin system. Earth Planet. Sci. Lett. 565, 116925 https://doi.org/10.1016/j.epsl.2021.116925.
Koroknai, B., Wórum, G., Tóth, T., Koroknai, Zs, Fekete-Németh, V., Kovács, G., 2020. Geological deformations in the Pannonian Basin during the neotectonic phase: New insights from the latest regional mapping in Hungary. Earth Sci. Rev. 211, 104311 https://doi.org/10.1016/j.earscirev.2020.103411.
Kovács, I., Falus, G., Stuart, G., Hidas, K., Szabó, C., Flower, M.F.J., Hegedűs, E., Posgay, K., Zilahi-Sebess, L., 2012. Seismic anisotropy and deformation patterns in upper mantle xenoliths from the central Carpathian–Pannonian region: Asthenospheric flow as a driving force for Cenozoic extension and extrusion? Tectonophysics 514, 168–179. https://doi.org/10.1016/j.tecto.2011.10.022.
Kovács, I., Patkó, L., Liptai, N., Lange, T.P., Taracsák, Z., Cloetingh, S.A.P.L., Török, K., Király, E., Karátson, D., Biró, T., Kiss, J., Pálos, Zs, Aradi, L.E., Falus, Gy, Hidas, K., Berkesi, M., Koptev, A., Novák, A., Wesztergom, V., Fancsik, T., Szabó, Cs, 2020. The role of water and compression in the genesis of alkaline basalts: Inferences from the Carpathian-Pannonian region. Lithos 354–355, 105323. https://doi.org/10.1016/j.lithos.2019.105323.
Le Corvec, N., Bebbington, M.S., Lindsay, J.M., McGee, L.E., 2013a. Age, distance, and geochemical evolution within a monogenetic volcanic field: Analyzing patterns in the Auckland Volcanic Field eruption sequence. Geochem. Geophys. Geosyst. 14 (9), 3648–3665. https://doi.org/10.1002/ggge.20223.
Le Corvec, N., Menand, T., Lindsay, J., 2013b. Interaction of ascending magma with pre-existing crustal fractures in monogenetic basaltic volcanism: an experimental approach. J. Geophys. Res. Solid Earth 118, 968–984. https://doi.org/10.1002/jgrb.50142.
Le Corvec, N., Spörli, K.B., Rowland, J., Lindsay, J., 2013c. Spatial distribution and alignments of volcanic centers: Clues to the formation of monogenetic volcanic fields. Earth Sci. Rev. 124, 96–114. https://doi.org/10.1016/j.earscirev.2013.05.005.
Liptai, N., Gráczer, Z., Szanyi, G., Cloetingh, S.A., Süle, B., Aradi, L.E., Falus, G., Bokelmann, G., Timkó, M., Timár, G., Szabó, C., 2022. Seismic anisotropy in the mantle of a tectonically inverted extensional basin: a shear-wave splitting and mantle xenolith study on the western Carpathian-Pannonian region. Tectonophysics 845, 229643. https://doi.org/10.1016/j.tecto.2022.229643.
Lorenz, V., 1986. On the growth of maars and diatremes and its relevance to the formation of tuff rings. Bull. Volcanol. 48, 265–274. https://doi.org/10.1007/bf01081755.
Magill, C.R., McAneney, K.J., Smith, I.E.M., 2005. Probabilistic Assessment of Vent Locations for the Next Auckland Volcanic Field Event. Math. Geol. 37, 227–242. https://doi.org/10.1007/s11004-005-1556-2.
Marcotte, S.B., Klepeis, K.A., Clarke, G.L., Gehrels, G., Hollis, J.A., 2005. Intra-arc transpression in the lower crust and its relationship to magmatism in a Mesozoic magmatic arc. Tectonophysics 407, 135–163. https://doi.org/10.1016/j.tecto.2005.07.007.

Marett, R., Emerman, S., 1992. The relations between faulting and mafic magmatism in the Altiplano-Puna plateau (Central Andes). Earth Planet. Sci. Lett. 112, 53–59. https://doi.org/10.1016/0012-821X(92)90006-H.

Martí, J., López, C., Bartolini, S., Becerril, L., Geyer, A., 2016. Stress controls of monogenetic volcanism: a review. Front. Earth Sci. 4, 106. https://doi.org/10.3389/feart.2016.00106.

Martin, U., Németh, K., 2004. Mio/Pliocene Phreatomagmatic Volcanism in the Western Pannonian Basin. Geologica Hungarica, Series Geologica, 26. Budapest.

Martin, U., Németh, K., Auer, A., Breitkreuz, C., 2003. Mio-Pliocene Phreatomagmatic Volcanism in a Fluvio-Lacustrine Basin in Western Hungary. Geolines 15, 84–90.

Matenco, L., Bertotti, G., Cloetingh, S.A.P.L., Dinu, C., 2003. Subsidence analysis and tectonic evolution of the external Carpathian-Moesian Platform region during Neogene times. Sediment. Geol. 156 (1–4), 71–94. https://doi.org/10.1016/S0037-0738(02)00283-X.

Mazzarini, F., 2007. Vent distribution and crustal thickness in stretched continental crust: the case of the Afar Depression (Ethiopia). Geosphere 3, 152–162. https://doi.org/10.1130/GES00070.1.

Mazzarini, F., Isola, I., 2010. Monogenetic vent self-similar clustering in extending continental crust: examples from the East African Rift System. Geosphere 6, 567–582. https://doi.org/10.1130/GES00569.1.

Mazzarini, F., Le Corvec, N., Isola, I., Favalli, M., 2016. Volcanic field elongation, vent distribution, and tectonic evolution of a continental rift: the Main Ethiopian Rift example. Geosphere 12, 706–720. https://doi.org/10.1130/GES01193.1.

Miller, R.H., 2015. Spatial Mapping of Strain patterns using GIS. In: Thesis for MS in Geology. Bowling Green State University, USA.

Nche, L.A., Hasegawa, T., Aka, F.T., Kobayashi, T., Németh, K., Asaah, A.N.E., Kaneda, Y., Nishihara, A., Bate-Tibang, E.E., Lebga, A.K., Tiabou, A.F., Ngwa, C.N., Suh, C.E., 2021. Lithostratigraphy and geochemistry of Aojiki volcano and Sumiyoshiike and Yonemaru maars, Kamo Volcanic Field (Southern Kyushu), Japan. J. Volcanol. Geotherm. Res. 412, 107170 https://doi.org/10.1016/j.jvolgeores.2020.107170.

Németh, K., 2010. Volcanic glass textures, shape characteristics and compositions of phreatomagmatic rock units from the Western Hungarian monogenetic volcanic fields and their implications for magma fragmentation. Central Eur. J. Geosci. 2 (3), 399–419. https://doi.org/10.2478/v10085-010-0015-6.

Németh, K., Martin, U., 1999. Late Miocene paleo-geomorphology of the Bakony-Balaton Highland Volcanic Field (Hungary) using physical volcanology data. Zeitschrift fr Geomorphol. 43 (4), 417–438.

Németh, K., Martin, U., 2007. Shallow sill and dyke complex in western Hungary as a possible feeding system of phreatomagmatic volcanoes in “soft-rock” environment. J. Volcanol. Geotherm. Res. 159, 138–152. https://doi.org/10.1016/j.jvolgeores.2006.06.014.

Németh, K., Korbély, B., Karátson, D., 2000. The Szigliget maar/diatreme, Bakony-Balaton Highland Volcanic Field. In: Terra Nostra, 6. International Maar Conference, Daun/Vulkaneifel, pp. 375–382.

Németh, K., Martin, U., Harangi, Sz, 2001. Miocene phreatomagmatic volcanism at Tihany (Pannonian Basin, Hungary). J. Volcanol. Geotherm. Res. 111, 111–135. https://doi.org/10.1016/S0377-0273(01)00223-2.

Norini, G., Baez, W., Becchio, R., Viramonte, J., Giordano, G., Arnosio, M., Pinton, A., Groppelli, G., 2013. The Calama–Olacapato–El Toro fault system in the Puna Plateau, Central Andes: Geodynamic implications and stratovolcanoes emplacement. Tectonophysics 608, 1280–1297. https://doi.org/10.1016/j.tecto.2013.06.013.

Porkoláb, K., Broerse, T., Kenyeres, A., Békési, E., Tóth, S., Magyar, B., Wesztergom, V., 2023. Active tectonics of the Circum-Pannonian region in the light of updated GNSS network data. Acta Geodaet. Geophys. https://doi.org/10.1007/s40328-023-00409-8.

Rodríguez, S.R., Morales-Barrera, W., Layer, P., Gonzálelz-Mercado, E., 2010. A quaternary monogenetic volcanic field in the Xalapa region, eastern Trans-Mexican volcanic belt: geology, distribution and morphology of the volcanic vents. J. Volcanol. Geotherm. Res. 197, 149–166. https://doi.org/10.1016/j.jvolgeores.2009.08.003.

Saint Blanquat, M., Tikoff, B., Teyssier, C., Vigneresse, J.L., 1998. Transpressional kinematics and magmatic arcs. In: Holdsworth, R.E., Strachan, R.A., Dewey, J.F. (Eds.), Continental Transpressional and Transtensional Tectonics, 135. Geological Society, London, Special Publications, pp. 327–340. https://doi.org/10.1144/GSL.SP.1998.135.01.21.

Schmid, S.M., Bernoulli, D., Fügenschuh, B., Matenco, L., Schefer, S., Schuster, R., Tischler, M., Ustaszewski, K., 2008. The Alpine-Carpathian-Dinaridic orogenic system: correlation and evolution of tectonic units. Swiss J. Geosci. 101, 139–183. https://doi.org/10.1007/s00015-008-1247-3.

Secomandi, M., Paoletti, V., Aiello, G., Fedi, M., Marsella, E., Ruggieri, S., D’Argenio, B., Rapolla, A., 2003. Analysis of the magnetic anomaly field of the volcanic district of the Bay of Naples, Italy. Mar. Geophys. Res. 24, 207–221. https://doi.org/10.1007/s11001-004-4220-1.

Seghedi, I., Downes, H., Vaselli, O., Szakács, A., Balogh, K., Pécskay, Z., 2004. Post-collisional Tertiary-Quaternary mafic alcalic magmatism in the Carpathian-Pannonian region: a review. Tectonophysics 393 (1–4), 43–62. https://doi.org/10.1016/j.tecto.2004.07.051.

Sheridan, M.F., Wohletz, K.H., 1983. Hydrovolcanism – basic considerations and review. J. Volcanol. Geotherm. Res. 17 (1–4), 1–29. https://doi.org/10.1016/0377-0273(83)90060-4.

Sieron, K., Juárez Cerrillo, S.F., González-Zuccolotto, K., Córdoba-Montiel, F., Connor, C. B., Connor, L., Tapia-McClung, H., 2021. Morphology and distribution of monogenetic volcanoes in Los Tuxtlas Volcanic Field, Veracruz, Mexico: implications for hazard assessment. Bull. Volcanol. 83, 47. https://doi.org/10.1007/s00445-021-01467-y.

Szabó, Cs, Harangi, Sz, Csontos, L., 1992. Review of Neogene and Quaternary volcanism of the Carpathian-Pannonian region. Tectonophysics 208 (1–3), 243–256. https://doi.org/10.1016/0040-1951(92)90347-9.

Szabó, Cs, Falus, Gy, Zajacz, Z., Kovács, I., Bali, E., 2004. Composition and evolution of lithosphere beneath the Carpathian–Pannonian Region: a review. Tectonophysics 393, 119–137. https://doi.org/10.1016/j.tecto.2004.07.031.

Tadini, A., Bonali, F.L., Corazzato, C., Cortés, J.A., Tibaldi, A., Valentine, G.A., 2014. Spatial distribution and structural analysis of vents in the Lunar Crater Volcanic Field (Nevada, USA). Bull. Volcanol. 76, 877. https://doi.org/10.1007/s00445-014-0877-8.

Tari, G., 1994. Alpine Tectonics of the Pannonian Basin. PhD Thesis,. Rice University, p. 9514233.

Tari, G., Horváth, F., 2010. Eo-Alpine evolution of the Transdanubian Range in the nappe system of the Eastern Alps: revival of a 15 years old tectonic model. Földtani Közlöny 140 (4), 483–510.

Tchamabé, B.C., Kereszturi, G., Németh, K., Carrasco-Núñez, G., 2016. How polygenetic are monogenetic volcanoes: case studies of some complex maar-diatreme volcanoes. In: Németh, K. (Ed.), Updates in Volcanology – From Volcano Modelling to Volcano Geology, pp. 355–389. https://doi.org/10.5772/63486.

Tibaldi, A., Pasquaré, F., Tormey, D., 2009. Volcanism in reverse and strike-slip fault settings. In: Cloething, S., Negendank, J. (Eds.), New Frontiers in Integrated Solid Earth Sciences, International Year of Planet Earth. Springer, Dordrecht. https://doi.org/10.1007/978-90-481-2737-5_9.

Török, K., 2012. On the origin and fluid content of some rare crustal xenoliths and their bearing on the structure and evolution of the crust beneath the Bakony–Balaton Highland Volcanic Field (W-Hungary). Int. J. Earth Sci. 101 (6), 1581–1597. https://doi.org/10.1007/s00531-011-0743-2.

Török, K., Dégi, J., Szép, A., Marosi, Gy, 2005. Reduced carbonic fluids in mafic granulite xenoliths from the Bakony-Balaton Highland Volcanic Field, Hungary. Chem. Geol. 223 (1–3), 93–108. https://doi.org/10.1016/j.chemgeo.2005.05.010.

Trippanera, D., Ruch, J., Acocella, V., Thordarson, T., Urbani, S., 2018. Interaction between central volcanoes and regional tectonics along divergent plate boundaries: Askja, Iceland. Bull. Volcanol. 80, 1. https://doi.org/10.1007/s00445-017-1179-8.

Ureta, G., Németh, K., Aguilera, F., Gonzalez, R., 2020. Features that Favor the Prediction of the Emplacement Location of Maar Volcanoes: a Case Study in the Central Andes, Northern Chile. Geosciences 10 (12). https://doi.org/10.3390/geosciences10120507.

Ureta, G., Németh, K., Aguilera, F., Zimmer, M., Menzies, A., 2021a. A window on mantle-derived magmas within the Central Andes: eruption style transitions at Cerro Overo maar and La Albondiga lava dome, northern Chile. Bull. Volcanol. 83 (4), 19. https://doi.org/10.1007/s00445-021-01446-3.

Ureta, G., Németh, K., Aguilera, F., Kósik, Sz, González, R., Menzies, A., González, C., James, D., 2021b. Evolution of a magmatic to a phreatomagmatic volcanic system: the birth of a monogenetic volcanic field, Tilocálar volcanoes, northern Chile. J. Volcanol. Geotherm. Res. 414, 107243 https://doi.org/10.1016/j.jvolgeores.2021.107243.

Uslular, G., Le Corvec, N., Mazzarini, F., Legrand, D., Gençalioğlu-Koşcu, G., 2021. Morphological and multivariate statistical analysis of quaternary monogenetic vents in the Central Anatolian Volcanic Province (Turkey): Implications for the volcano-tectonic evolution. J. Volcanol. Geotherm. Res. 416, 107280 https://doi.org/10.1016/j.jvolgeores.2021.107280.

Valentine, G.A., Gregg, T.K.P., 2008. Continental basaltic volcanoes; processes and problems. J. Volcanol. Geotherm. Res. 177 (4), 857–873. https://doi.org/10.1016/j.jvolgeores.2008.01.050.

Valentine, G.A., Perry, F.V., 2007. Tectonically controlled, time-predictable basaltic volcanism from a lithospheric mantle source (central Basin and Range Province, USA). Earth Planet. Sci. Lett. 261, 201–216. https://doi.org/10.1016/j.epsl.2007.06.029.

Vauchez, A., Tommasi, A., Mainprice, D., 2012. Faults (shear zones) in the Earth's mantle. Tectonophysics 558, 1–27. https://doi.org/10.1016/j.tecto.2012.06.006.

Visnovitz, F., Jakab, B., Czecze, B., Hámori, Z., Székely, B., Fodor, L., Horváth, F., 2021. High resolution architecture of neotectonic fault zones and post-8-Ma deformations in western Hungary: Observations and neotectonic characteristics of the fault zone at the Eastern Lake Balaton. Glob. Planet. Chang. 203, 103540 https://doi.org/10.1016/j.gloplacha.2021.103540.

von Veh, M.W., Németh, K., 2009. An assessment of the alignments of vents on geostatistical analysis in the Auckland Volcanic Field, New Zealand. Geomorphol. Relief, Processus, Environ. 3, 175–186. https://doi.org/10.4000/geomorphologie.7664.

Walker, G.P.L., 1993. Basaltic-volcano systems. In: Prichard, H.M., Alabaster, T., Harris, N.B.W., Nearly, C.R. (Eds.), Magmatic Processes and Plate Tectonics. Geological Society. Special Publications, London, pp. 3–38. https://doi.org/10.1144/GSL.SP.1993.076.01.01.

Watanabe, T., Koyaguchi, T., Seno, T., 1999. Tectonic stress controls on ascent and emplacement of magmas. J. Volcanol. Geotherm. Res. 91, 65–78. https://doi.org/10.1016/S0377-0273(99)00054-2.

Wéber, Z., 2018. Probabilistic joint inversion of waveforms and polarity data for double-couple focal mechanisms of local earthquakes. Geophys. J. Int. 213 (3), 1586–1598. https://doi.org/10.1093/gji/ggy096.

Wijbrans, J., Németh, K., Martin, U., Balogh, K., 2007. $^{40}Ar/^{39}Ar$ geochronology of Neogene phreatomagmatic volcanism in the western Pannonian Basin, Hungary. J. Volcanol. Geotherm. Res. 164, 193–204. https://doi.org/10.1016/j.jvolgeores.2007.05.009.

Wórum, G., Koroknai, B., Koroknai, Zs, Fekete-Németh, V., Kovács, G., Tóth, T., 2020. Young Geological Deformations in Hungary. Geomega Ltd., Budapest https://doi.org/10.17632/dnjt9cmj87.1.